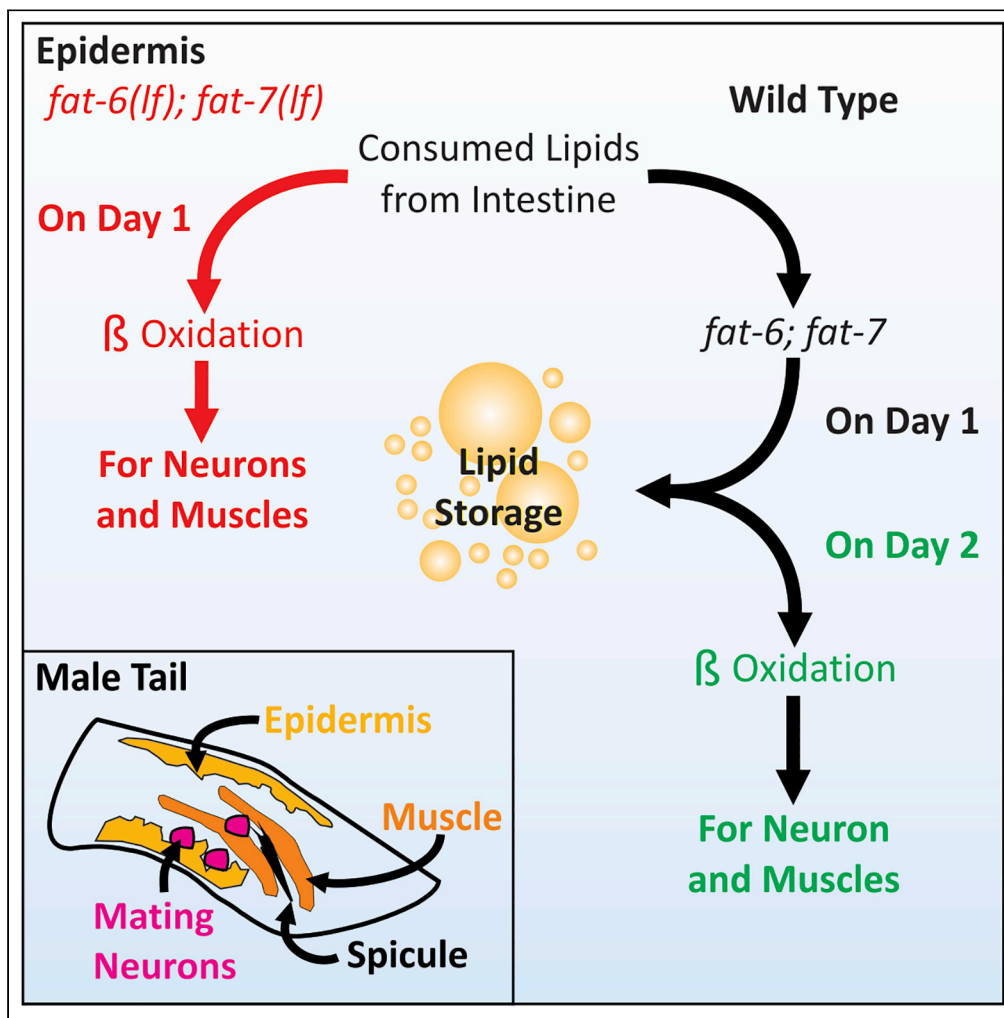**Article**

Stearoyl-CoA desaturases sustain cholinergic excitation and copulatory robustness in metabolically aging *C. elegans* males

Jimmy Goncalves, Yufeng Wan, L. René Garcia

rgarcia@bio.tamu.edu

Highlights

Tissue distribution of *fat-6*-encoded stearoyl-CoA desaturase changes in adulthood

Markov modeling shows reduced feeding linked with more exploring in day 2 males

fat-6(*lf*); *fat-7*(*lf*) disrupted behavior can be rescued by epidermal FAT-6

fat-6(*lf*); *fat-7*(*lf*) alters neural and muscular ERG and EAG K+ channel expression

Article

Stearoyl-CoA desaturases sustain cholinergic excitation and copulatory robustness in metabolically aging *C. elegans* males

Jimmy Goncalves,[1] Yufeng Wan,[1] and L. René Garcia[1,2,*]

SUMMARY

Regulated metabolism is required for behaviors as adults age. To understand how lipid usage affects motor coordination, we studied male *Caenorhabditis elegans* copulation as a model of energy-intensive behavior. Copulation performance drops after 48 h of adulthood. We found that 12–24 h before behavioral decline, males prioritize exploring and copulation behavior over feeding, suggesting that catabolizing stored metabolites, such as lipids, occurs during this period. Because *fat-6/7*-encoded stearoyl-CoA desaturases are essential for converting the ingested fatty acids to lipid storage, we examined the copulation behavior and neural calcium transients of *fat-6(lf); fat-7(lf)* mutants. In wild-type males, intestinal and epithelial *fat-6/7* expression increases during the first 48 h of adulthood. The *fat-6(lf); fat-7(lf)* behavioral and metabolic defects indicate that in aging wild-type males, the increased expression of stearoyl-CoA desaturases in the epidermis may indirectly modulate the levels of EAG-family K$^+$ channels in the reproductive cholinergic neurons and muscles.

INTRODUCTION

Cognitive and locomotor processes controlling behavior decline with age. However, behavioral decline can be modified by genetics, diet, and the environment (Carlsson, 2010; Liu and Zhang, 2014; Ochoa et al., 2011; Solomon et al., 2009). For example, neuronal function, which regulates behavior, has been shown to be directly affected by metabolic perturbation including lipid-based inflammation and oxidative stress (Wu et al., 2012). Specifically, dyslipidemia–atypical amounts of lipids in the brain–contributes to disrupted mitochondrial motility and biosynthesis, increased respiration, and higher ATP turnover, leading to excess radical production (Ochoa et al., 2011). In neurodegenerative disease, mitochondrial disruption and excess radical production have been implicated in exacerbating dysfunction. In addition, diets emphasizing reduced intake of saturated fats have been correlated with decreased cognitive decline, suggesting there may exist metabolic mechanisms involved in neuronal performance (Amtul et al., 2011; Appel et al., 2005; Tangney et al., 2014).

Caenorhabditis elegans virgin males grown in laboratory conditions decline in mating behavior during the first 3–5 days of adulthood, despite having a median lifespan of ~10 days (Gems and Riddle, 2000). Rapid male mating behavior decline suggests physiological changes are taking place in which neuromuscular function is compromised (Guo et al., 2012). The aforementioned phenomena precede any morphological decay seen in older animals. For example, muscle degradation is observed by day 8 of adulthood, sperm activation is undisrupted by day 5 of adulthood, and the nervous system remains unchanged by day 4 of adulthood (Cohn et al., 2020; Glenn et al., 2004; Herndon et al., 2002).

Behavioral decay in aging *C. elegans* males is affected by changes in metabolism and neuromuscular excitability. Specifically, the copulatory neurons and muscles of 72-h adult males are hyper-excited, showing increases in calcium transients and sensitivity to acetylcholine agonist stimulation (Guo et al., 2012). Behavioral decay can be modulated by transient food deprivation, inducing *daf-2*-dependent CAMKII/UNC-43 phosphorylation of EAG/EGL2 K$^+$ channels that hyperpolarize excitable cells (LeBoeuf et al., 2007, 2011). Transient starvation can also induce metabolic adaptations to overcome the behavioral decline associated with aging.

[1]Department of Biology, Texas A&M University, College Station, TX 77843, USA

[2]Lead contact

*Correspondence: rgarcia@bio.tamu.edu

Metabolism's role in behavioral decline has been studied in a mutant of *sir-2.1*, a NAD-dependent deacetylase that regulates metabolic gene expression. Mutant males of *sir-2*.1 prematurely decline in mating behavior due to dysregulated glycolytic and fatty acid oxidation catabolic processes. The alterations in metabolism lead to excessive production of ROS, which disrupts calcium handling and damages biomolecules, and exacerbates behavioral dysfunctions associated with age (Guo and García, 2014). To address how metabolic adaptations counteract enhanced catabolism, we queried metabolic gene expression in aging males. Phosphoenolpyruvate carboxykinase (PEPCK), an enzyme involved in gluco-/glyceroneogenesis, and stearoyl-CoA desaturases (SCD) enzymes used for fat synthesis were found to increase within the first 48 h of adulthood in wild-type males. Epidermal PEPCK was observed to sustain the neuromuscular circuitry during early to mid-adulthood, partially by maintaining *egl-2*-encoded *ether-a-go-go* K$^+$ channel expression (Goncalves et a.l., 2020). Despite the correlation between increased glycolytic and fatty acid oxidation and altered behavioral decline, it remains unknown if metabolic changes are a cause or a compensatory mechanism for declining behavior. To understand how fuel utilization affects neuronal activity, we studied the contributions of stearoyl-CoA desaturases on fatty acid metabolism, behavioral states, and neuromuscular system performance.

Stearoyl-CoA desaturases (SCD), encoded by *fat-5, fat-6,* and *fat-7*, catalyze the rate limiting step of monounsaturated fatty acid synthesis. Both *fat-6* and *fat-7* primarily desaturate stearic acid (C18:0) producing oleic acid (C18:1); *fat-5* differs in that palmitic acid (C16:0) is desaturated to palmitoleic acid (C16:1) (Watts and Browse, 2000). Mutants of *fat-6* and *fat-7* are therefore suggested to be deficient for synthesizing triacylglycerides, composed of C16:1 and C18:1, for storage and accumulating fatty acids (Vrablik et al., 2015). In hermaphrodites, the low fat phenotype of *fat-6*(*lf*)*; fat-7*(*lf*), coupled with increased mRNA of a predicted acyl-CoA synthetase (*acs-2*) and a β-oxidation enzyme (*ech-1*),supports the hypothesis that mutants may also undergo enhanced mitochondrial beta oxidation, in addition to their defect in triacylglyceride storage (Brock et al., 2007). However, the low fat phenotype of *fat-6*(*lf*)*; fat-7*(*lf*) animals can be ameliorated by depleting the nuclear hormone receptor NHR-64, causing an increase in the expression of *pod-2*, which encodes an acetyl-CoA carboxylase that catalyzes a rate limiting step of fatty acid biosynthesis, and also a decrease in the expression of *acox-1.4*, which is involved in peroxisome-based fat oxidation (Liang et al., 2010).

In this work we sought to understand how lipid metabolism promotes male mating behavioral fitness and sustains copulation ability. We postulate that during the first two days of male adulthood, physiological changes take place in the epithelia and intestine to support the copulatory neuromuscular circuitry. Of the physiological changes, we sought to determine why *fat-6* mRNA is up-regulated during this period. We found that wild-type males' feeding behavior decreases after the first 24 h of adulthood. Despite changes in feeding, mating performance is maintained during the first 48 h of adulthood, likely through the usage of internal lipid stores generated during the first 24 h of adulthood. To study the consequences of dysregulated fatty acid oxidation and lipid storage deficiency during the first 24 h of adulthood, we studied the copulation behavior and neuromuscular activities of *fat-6*(*lf*)*; fat-7*(*lf*)mutant males. Our work with the double mutants suggests that in aging wild-type males, the changing levels of stearoyl-CoA desaturases in the epidermis non-cell-autonomously modulate pre- and post-synaptic K$^+$ channel mRNA expression, which may sustain the function of reproductive cholinergic motor circuits.

RESULTS

Tissue-specific FAT-6 changes during the first two days of male adulthood

In an earlier study, metabolic changes in the male *C. elegans* were found to sustain copulation behavior during the first two days of adulthood (Guo and García, 2014; Guo et al., 2012). RT-qPCR analysis of metabolic gene expression was conducted on day 1 and day 2 adult males (Guo and García, 2014). Of the genes queried, the stearoyl-CoA desaturase genes *fat-5/6/7*, involved in lipid synthesis, showed a 3- to 9-fold increase in expression. Here, we confirmed the changes in stearoyl-CoA desaturase gene expression with 8-15 biological replicates, each containing pooled transcripts of three males. Both *fat-5* and *fat-6* RNA significantly increased from day 1 to day 2 of adulthood; *fat-7* RNA is marginally elevated on day 2 but not with statistical significance (Figure 1A). The slight change in *fat-7* levels may be explained by its redundant function with *fat-6* (Watts and Browse, 2000).

Since the gene expression of stearoyl-CoA desaturase, also known as Δ9 fatty acid desaturase, increases in aging males, we asked how the protein levels correlated with mRNA amounts. FAT-6 protein was visualized
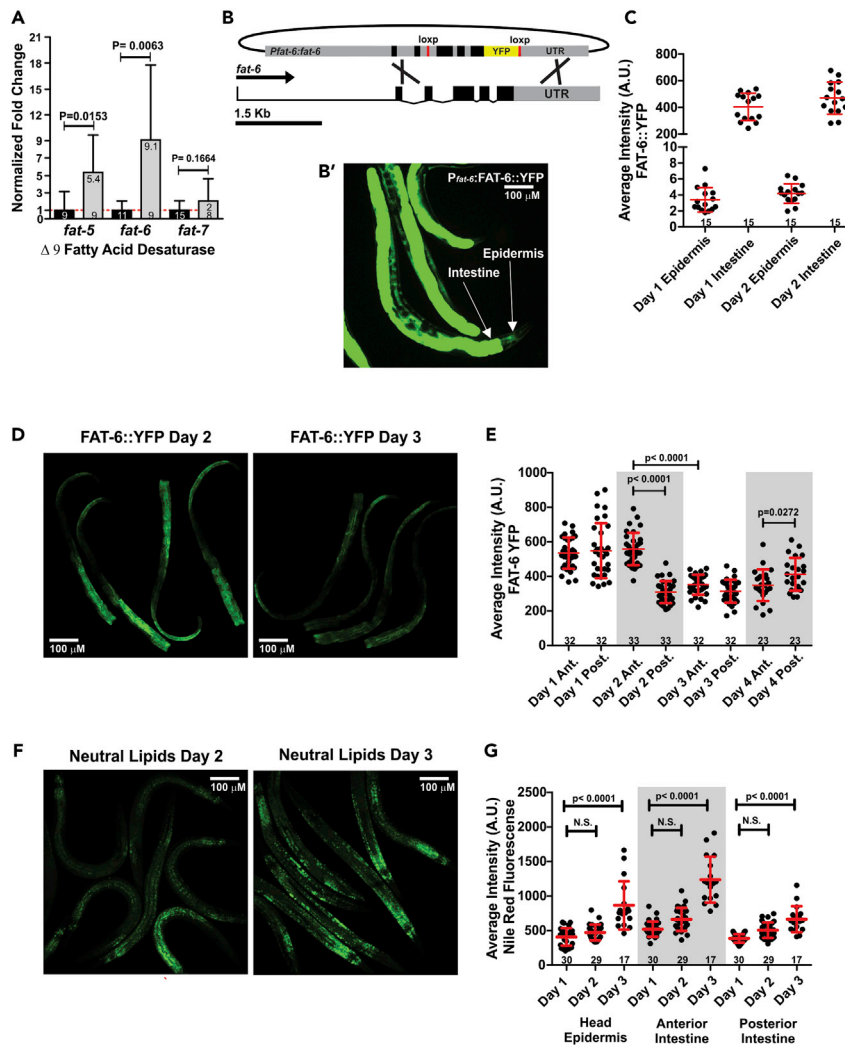
Figure 1. FAT-6:YFP expression in Aging Males

(A) RT-qPCR results of stearoyl CoA desaturases *fat-5*, *fat-6* and *fat-7* in day 1 (black columns) and day 2 (gray columns) wild-type adult males (3 males/replicate). Each individual gene was normalized to the day 1 equivalent. Numbers of independent biological replicates assayed are listed below the data. Error bars represent SD. p values were determined using the unpaired t-test.

(B and B') Cartoon of CRISPR/Cas9 FAT-6:YFP knock-in design and confocal images of FAT-6:YFP expression in adult hermaphrodites; panel shows whole worm intestinal and head epidermal expression.

(C) FAT-6:YFP fluorescence in day 1 and day 2 males was quantified by a series of rectangular ROIs drawn over the epidermis and intestine.

(D) Intestinal FAT-6:YFP fluorescence in aging wild-type males.

(E) FAT-6:YFP fluorescence in panel (D), was quantified by a series of rectangular ROIs drawn over the intestine; the series of ROIs corresponding to the first half of the intestine were designated anterior. The posterior was composed of the second half of the intestine extending to the end of the male body. p values were determined using one-way ANOVA with Bonferroni's multiple comparisons after test.

(F) Fixative Nile Red staining of aging wild-type males.

(G) Fixative Nile red staining in (F) was quantified by a series of rectangular ROIs drawn over the epidermis and intestine. p values were determined using one-way ANOVA with Bonferroni's multiple comparisons posttest. For (C), (E) and (G), bars and whiskers represent mean and SD. Numbers of animals assayed are listed at the bottom. A.U. (Arbitrary Units).

using a CRISPR/Cas9 generated YFP and loxP-flanked knock-in (see STAR Methods) (Figure 1B). We observed epidermal and intestinal FAT-6:YFP expression throughout larval development and into hermaphrodite and male adulthood (Figures 1B' and S1A–S1E). FAT-6:YFP head epidermal signals (Figures S1B and S1C) were ~1% of that seen in the intestine of adult males (Figure 1C) and hermaphrodites

(Figure 1B'). This observation differed from published work in which a *fat-6*:GFP transgene displayed strong expression in the epidermis throughout all life stages (Brock et al., 2006). Differences may be due to changes in transcriptional or translational regulation, as the earlier published transgene only included a ~2.6 kb upstream regulatory region, the first exon, and part of the second exon (Brock et al., 2006). To confirm the FAT-6:YFP CRISPR/Cas9 allele was functioning similar to wild-type FAT-6, we introduced the knock-in into a *fat-7(lf)*mutant and visualized intestinal neutral lipid storage using fixative fluorescent Nile Red staining.

Nile Red can indirectly distinguish hydrophobic membrane proteins, polar lipids, and neutral lipids. Its 630 nm (red) emission maximum stains cellular hydrophobic membrane proteins and polar lipids when excited by 550- 560 nm light. Whereas when staining neutral lipid droplets, Nile Red's excitation/emission spectra blue-shifts; its 520 nm–560 nm (green) emission can be visualized by excitation with 480–520 nm light (Fowler and Greenspan, 1985; Greenspan et al., 1985). In *C. elegans*, lipid droplets are cytoplasmic organelles containing triacylglycerides (TAGs) composed of the Δ9 fatty acid desaturase products C16:1 and C18:1 (Vrablik et al., 2015). The fixative procedure for staining worms with Nile Red destroys the fluorescence of YFP, allowing visualization of the Nile Red fluorescence. If FAT-6 was compromised by the YFP, then in a *fat-7(lf)* mutant background, the male will have a low 514 nm excitation/540 nm emission (hence referred to as Ex514/Em540) Nile Red staining, suggesting reduced neutral lipid stores. We observed in *fat-6(lf); fat-7(lf)* males a 68% decrease in Ex514/Em540 Nile Red fluorescence (Figures S2A and S2A'), similar to what was published for *fat-6(lf); fat-7(lf)* mutant hermaphrodites (Brock et al., 2007). In contrast, we observed similar Ex514/Em540 Nile Red fluorescence intensities of whole intestine in wild-type males, *fat-6*:YFP males and *fat-6*:YFP males that also contain the *fat-7(lf)* single and *fat-7(lf)*, *fat-5(lf)* double mutations (Figures S2A'–S2D). Fixative Oil Red O is another fat soluble dye that stains lipo-proteins, neutral and polar lipids (Escorcia et al., 2018; Fowler and Greenspan, 1985). It stains neutral lipid droplets red, which can be visualized by standard light microscopy. Similar to fixative Nile Red staining, quantification of fixative Oil Red O staining in *fat-6*:YFP; *fat-7(lf)* males was similar to wild-type males, suggesting FAT-6 function was not compromised by translational fusion with the YFP protein (Figure S2A'').

Contrary to the accumulation of *fat-6* transcripts in aging males, FAT-6:YFP fluorescence levels decreased with age in segments of the intestine (Figures 1D and 1E). In aging males, the anterior intestine remained unchanged during days 1-2 of adulthood (Figures 1D and 1E). However, declines in the anterior intestine were observed during day 3 of adulthood (Figures 1D and 1E). The posterior intestinal FAT-6:YFP, next to the gonadal seminal vesicle (spermatid storage) and vas deferens, decreased earlier from day 1-2 of adulthood (Figures 1D and 1E). Attenuation of posterior intestinal FAT-6 might suggest a need for the desaturase to support reproductive functions. Although FAT-6:YFP intensity decreased in the posterior intestine with age, we observed continual Ex514/Em540 Nile Red fluorescent staining in the head epidermis and intestine during day 1 and 2, and a slight increase during day 3. This data suggests that although there is a decrease in FAT-6:YFP fluorescence, there is sufficient stearoyl-CoA desaturase activity during the three days of adulthood (Figures 1F and 1G).

Since the middle-posterior intestine, which is next to the germline and somatic gonad, showed differential FAT-6:YFP fluorescence with age, we asked if posterior intestinal FAT-6 is responsive to the male's reproductive system. To determine the gonad's role in the regulation of intestinal FAT-6, germline and somatic gonad precursor cells in early L1 males were laser-ablated, and FAT-6:YFP was quantified in day 1 and day 2 adults (Figure S2E). In day 1 and day 2 males, FAT-6:YFP fluorescent levels in the anterior and intermediate (middle) intestine were similar between the control and gonad-ablated males. However, in day 2 gonad-ablated males, the posterior-most intestine (Figure S2E') showed further decreased FAT-6:YFP fluorescence. This observation suggests that the male gonad (possibly the vas deferens of the somatic gonad) indirectly regulates the expression of *fat-6* in the posterior intestine.

Lipid mobilization can occur in the absence of FAT-6/7

In *C. elegans*, others have shown that triacylglycerides (TAGs) are composed of hydrocarbon chains that can be acquired from bacterially-ingested saturated fat. *E. coli*, a laboratory food for *C. elegans*, primarily provides lipids in the form of palmitic acid, a saturated 16 carbons long (16:0) fat (Tanaka et al., 1996). FAT-5/6/7 can desaturate C16:0 to C16:1 (Watts and Browse, 2000).Additionally, FAT-6/7 can also desatu-rate C18:0 to C18:1 (Watts and Browse, 2000) to create the rate limiting precursors, mono-unsaturated fatty acids, for TAGs. The final composition of a TAG can consist of C16:0, C16:1, C18:0, and/or C18:1 dietary and

self-synthesized lipids (Perez and Van Gilst, 2008; Srinivasan, 2015). However, the reduced fixative Ex514/Em540 Nile Red fluorescence of *fat-6(lf); fat-7(lf)* males suggests that in the mutant, TAGs containing solely of C16:0 are inefficiently formed or readily metabolized. This raises the question of how ingested palmitic acid from bacteria affects an adult male that has a deficiency in Δ9 fatty acid desaturase activity.

Although FAT-6/7 promotes neutral lipid storage, and we observed decrease in Ex514/Em540 Nile Red fluorescence in *fat-6(lf); fat-7(lf)* males (Figures S2A and S2A'), it is possible the Nile Red staining was affected by something else unrelated to reduced stearic acid desaturation. FAT-6/7 are specifically required to desaturate stearic acid (18:0) to the unsaturated fat oleic acid (18:1n-9) (Watts and Browse, 2000). To establish whether decreased fixative Nile Red fluorescence in *fat-6(lf); fat-7(lf)* was due to a lack of stearic acid desaturation, we artificially supplemented the mutant's diet with exogenous oleic acid, similar to previous work with hermaphrodites (via *E. coli* OP50 containing oleic acid, see methods (Brock et al., 2007; Deline et al., 2013; Shi et al., 2013)). Oleic acid supplementation should increase TAG stores in wild-type males (as reported in hermaphrodites (Han et al., 2017)) and restore intestinal TAG stores in *fat-6(lf); fat-7(lf)* mutant males, which can be indirectly detected by increased fixative Ex514/Em540 Nile Red fluorescence.

Artificial oleic acid supplementation increased fixative Ex514/Em540 Nile Red fluorescence in both day 1 adult *fat-6(lf); fat-7(lf)* and wild-type males, relative to males fed the standard diet (Figure 2A). Although intestinal lipid droplets were restored by exogenous oleic acid supplementation, we did not know how dynamic these lipid droplets would be in day 2 and 3 *fat-6(lf); fat-7(lf)* mutant males. We removed oleic acid from the mutant's diet (by acutely switching the male's diet to OP50 bacteria that does not contain oleic acid) and asked if fixative Nile Red fluorescence was reduced due to stored lipid utilization. However, in day 2 and day 3 mutant males, we unexpectedly observed that intestinal Nile Red fluorescence was higher than day 1 (Figure 2A).Since the stearoyl-CoA desaturase activities are greatly reduced and the remaining FAT-5 provides minimal lipid storage in *fat-6(lf); fat-7(lf)* males, we do not believe that new synthesis of C16:1 and C18:1 is likely responsible for fluorescence increases after removal of oleic acid-containing bacteria. Although we did not measure lipid mobilization directly, lipids might be trafficked from other regions back to the intestine, followed by lipid redistribution and usage. Additionally, polyunsaturated fatty acids could be mobilized and incorporated into new TAG's, resulting in day 2 increased intestinal lipid storage.

Similar to *fat-6(lf); fat-7(lf)*, in wild-type males, oleic acid-supplementation until day 1 adulthood also showed huge increase in Nile Red fluorescence, which continued into all three days of adulthood (Figure 2A). This observation is not unexpected and suggests that augmenting an *ad libitum* diet with excess mono-unsaturated lipids can alter neutral lipid stores in animals with functioning Δ9 fatty acid desaturase. Altogether, the change of oleic acid metabolism in *fat-6(lf); fat-7(lf)* males indicates that if there is an interruption in unsaturated fat synthesis, lipids can be trafficked from other tissues to the intestine.

Stearoyl-CoA desaturase mutants display higher oxygen consumption than wildtype

The *fat-6(lf); fat-7(lf)* mutants develop slowly despite continually ingesting bacterially-derived saturated fat (C16:0) (Brock et al., 2006).Since it is crippled for storing neutral lipids, the male might use the ingested fatty acids, or their hydrolytic products, for immediate anabolic processes including, but not limited to providing acyl chains for phospholipids production. Although excess could be lost through excretion/defecation, it might also perturb oxidative catabolism. Thus we asked if the disruption in *fat-6(lf); fat-7(lf)* metabolism and physiology can be measured through altered oxygen consumption. β-oxidation of short ($<C_8$), medium (C_8-C_{12}), and long chain fatty acids (C_{14}-C_{20}) predominantly occurs in the mitochondria (Reddy and Hashimoto, 2001). Peroxisomes can functionally complement the mitochondria with the β-oxidation of long chain fatty acids (C_{14}-C_{20}). Therefore, palmitic acid (C16:0) can be metabolized by peroxisomes into medium chain fatty acids (C_8-C_{12}), which are then transported to the mitochondria (Reddy and Hashimoto, 2001). However given the exclusive ability of peroxisomes to catabolize very long fatty acids ($>C_{20}$), we expect mitochondrial β-oxidation to primarily oxidize bacterially-derived palmitic acid (16:0) (Reddy and Hashimoto, 2001; Tanaka et al., 1996).

To address if oxygen consumption of *fat-6(lf); fat-7(lf)* males is altered compared to wild-type males, we put well-fed day 1 wild-type and *fat-6(lf); fat-7(lf)* males in S-basal solution (a common worm culture buffer) that contains an oxygen-sensitive electrode. A measured increase in voltage change, which corresponds to decreasing oxygen in the solution, is an indirect measure of respiration. We observed that day 1 *fat-6(lf)*;
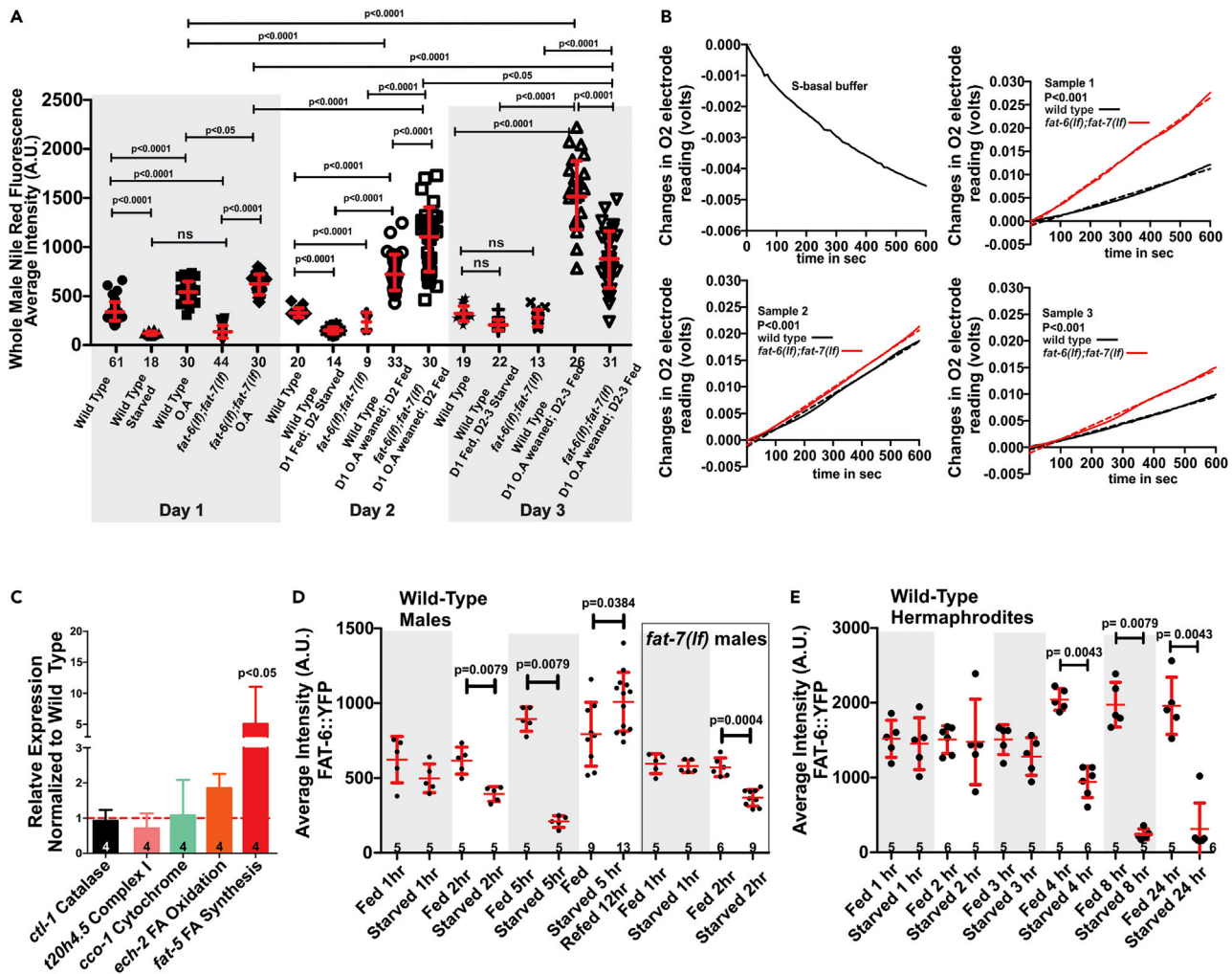
Figure 2. Metabolic Characterization of *fat-6*(*lf*); *fat-7*(*lf*) males

(A) Fixative Nile Red fluorescence quantification of day 1-3 males that were either starved or grown with and without oleic acid (O.A)-fed bacteria. O.A supplemented males were grown from eggs to day 1 adult males on agar plates that contain OP50 bacteria fed with 0.3 mM oleic acid. To wean the males from oleic acid, males were moved to agar plates that contained OP50 bacteria that were not fed with oleic acid; day 2 males were weaned off oleic acid for 24 h, and day 3 males were weaned off oleic acid for 48 h. For day 1 starved males, well-fed L4 males were washed of bacteria and then placed on 100 μg/mL ampicillin agar plates that lack bacterial food and assayed as adults 24 h later. For day 2 and day 3 starved males, day 1 well-fed males were washed of bacteria and then placed on 100 μg/mL ampicillin agar plates for 24 and 48 h that lack bacterial food. p values for daily comparisons, and separately between days, were determined using one-way ANOVA with Bonferroni's multiple comparison posttest.

(B) Oxygen consumption of S-basal buffer and 50 males in S-basal buffer per independent sample, as measured by change in voltage over time (10 min). N= 3 independent paired samples of wildtype and *fat-6*(*lf*); *fat-7*(*lf*) day 1 males. Solid lines are measured data; fitted dashed lines were determined by linear regression. The slopes of fitted lines of *fat-6*(*lf*); *fat-7*(*lf*) oxygen consumption is steeper than wildtype in all three trials. p values (determined in Prism) represent the chance of the slopes from the fitted lines being identical.

(C) RT-qPCR results, one male per biological replicate, of the metabolic genes *ctl-1*, *T20H4.5*, *cco-1*, *ech-2*, and *fat-5*. Error bars represent SD. p values were determined using the Kruskal-Walis test. Number of biological replicates are listed below the bars.

(D and E) Intestinal FAT-6:YFP expression. Starved animals were grown on NGM plates lacking OP50; a glycerol ring around the edge of the agar was used to contain animals on the NGM plate. p values were determined using the unpaired t-test. Bars and whiskers represent mean and SD. Number of animals assayed are listed below data. A.U. (Arbitrary Units).

fat-7(*lf*) males consume more oxygen than wild-type males (3 independent trials, 50 males per trial) (Figure 2B). This observation suggests that the deficiency in storing lipids has secondary effects such as over-catabolism or possibly inappropriate free fatty acid-mediated activation of uncoupling protein 1 (UCP1), which is known to induce mitochondrial proton leak and promote oxygen consumption (Woyda-Ploszczyca and Jarmuszkiewicz, 2017).
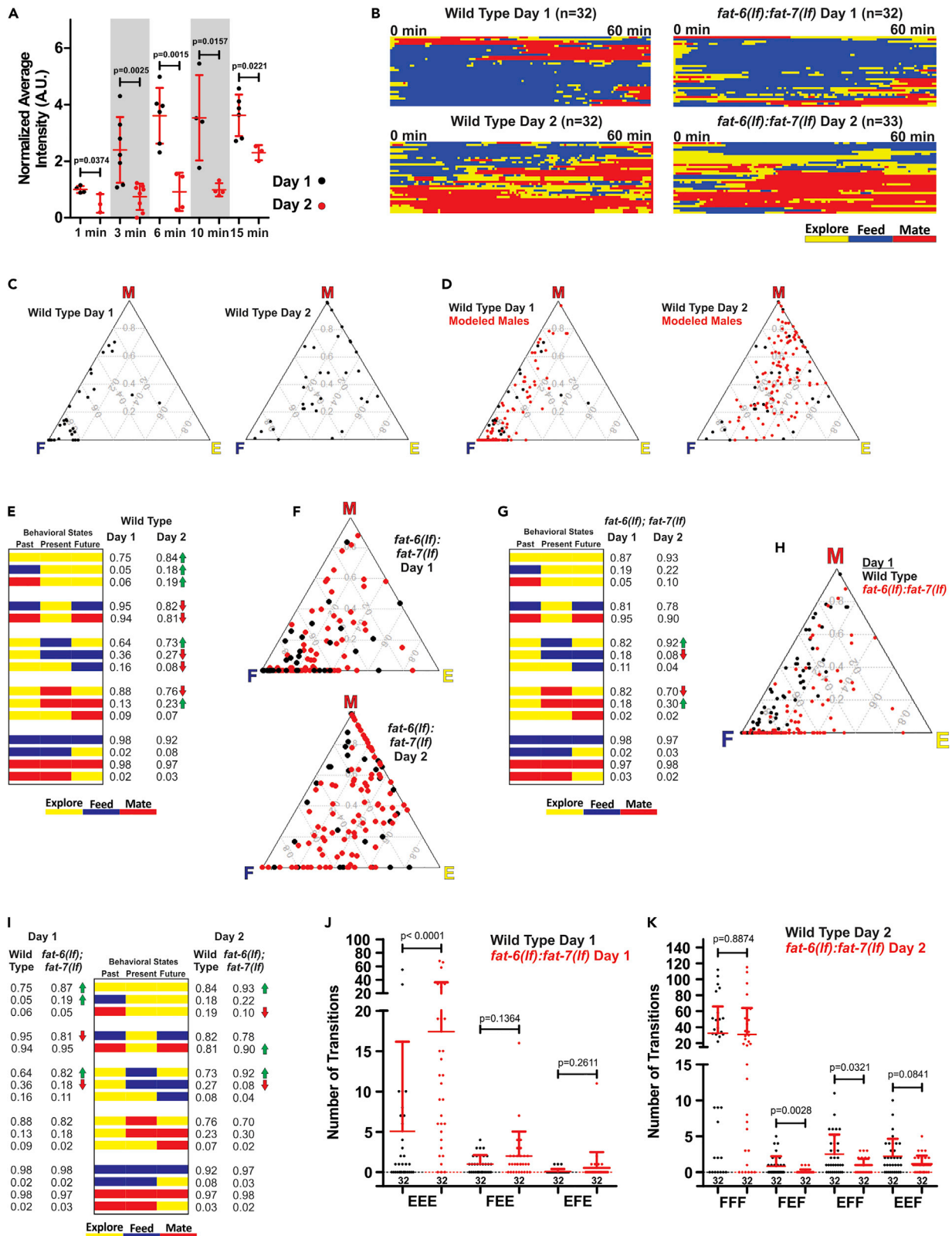
Figure 3. Age-dependent behavioral choice in male *C. elegans*

(A) The bacterial consumption rate of aging wild-type males quantified by fluorescence OP50 within the intestinal lumen. Bars and whiskers represent mean and SD. p values were determined using the unpaired t-test.

(B) Raw data stacks of male choice behaviors colorized in yellow, blue, and red for exploring, feeding, and mating behaviors, respectively. Stacks consist of 32 bior tricolored horizontal lines each depicting the duration of exploring, feeding, and mating behaviors of a single male over the time course of 1 h.

(C) The average proportion of time spent on exploring (E), feeding (F), and mating (M) behavior is plotted as a ternary graph, and each data point is an individual male. As a data point reaches a vertex, the proportion approaches 1. A data point localized to a vertex represents 1 h of performing a single behavior.

(D) Markov-simulated data is depicted in red and co-plotted with the raw data in black.

(E) A Markov model state diagram of aging wild-type males shows an age-specific proportion, the probability of transitioning to a future state based on its present and past state, colorized in yellow, blue, and red for exploring, feeding, and mating behaviors. The green upward arrows adjacent to day 2 proportions represent increases in day 2 proportions when compared to day 1. The red downward arrow adjacent to day 2 proportions represents decreases in day 2 proportions when compared to day 1.

(F) *fat-6(lf); fat-7(lf)* Markov-simulated data in red is depicted and co-plotted with the raw data in black.

(G) A Markov model state diagram, of aging *fat-6(lf); fat-7(lf)* males, shows an age-specific proportion, the probability of transitioning to a future state based on its present and past state, colorized in yellow, blue, and red for exploring, feeding, and mating behaviors. The green upward arrows adjacent to day 2 proportions represent increases in day 2 proportions when compared to day 1. The red downward arrow adjacent to day 2 proportions represents decreases in day 2 proportions when compared to day 1.

(H) Markov-simulated data for wildtype in black and *fat-6(lf); fat-7(lf)* in red on day 1 of adulthood.

(I) A Markov model state diagram comparing aging wild-type and *fat-6(lf); fat-7(lf)* males from (E) and (G).

(J) The number of behavioral transitions leading to exploring, as a future state, in day 1 adults. The behavioral transitions across age were quantified from observed data in (B). *P*-values determined using the Mann Whitney non-parametric test.

(K) The number of behavioral transitions leading to feeding, as a future state, in day 2 adults. The behavioral transitions across age were quantified from observed data in (B). *P*-values determined using the Mann Whitney non-parametric test. A.U. (Arbitrary Units).

Because *fat-6(lf); fat-7(lf)* mutants showed increased oxygen consumption, we performed RT-qPCR to query expression changes in other metabolic genes. Since there are three stearoyl-CoA desaturase genes, we expect the remaining desaturase gene, *fat-5*, to be upregulated in the double mutant. In addition, if the double mutant over-catabolize saturated fat and respiration increases as a result, then we might also observe expression changes in genes such as *ctl-1* (catalase, which coverts H_2O_2 to water and oxygen), T20H4.5 (NADH dehydrogenase, which is part of the electron transport complex), *cco-1* (cytochrome *c* oxidase) and *ech-2* (enoyl-CoA hydratase, which is involved in β-oxidation). Not surprisingly, we measured significant increases in *fat-5* by ∼4-fold, which is similar to previous reports for hermaphrodites (Figure 2C) (Brock et al., 2007). However, we did not measure significant increases in the other genes involved in fatty acid oxidation, despite *ech-2* being marginally elevated. This observation indicates that not all facets of metabolism were transcriptionally adjusted to the animal's altered physiology.

Since the stearoyl-CoA desaturases balance the storage and catabolism of lipids, we asked whether acute changes in feeding can also regulate FAT-6 levels. Chronic starvation caused fixative Nile Red staining in wild–type males to drop (Figure 2A), thus we measured the levels of FAT-6:YFP under starvation conditions. We found that regardless of *fat-7*, 2 h of starvation reduces FAT-6:YFP fluorescence in day 1 adult males, suggesting rapid protein degradation triggered by starvation (Figure 2D). Wild-type hermaphrodites also showed fluorescent decline of FAT-6:YFP, but after 4 h since food removal (Figure 2E). The dimorphic difference is likely due to hermaphrodites starting with 3 times higher FAT-6:YFP during day 1 of adulthood (Figures 2D and 2E). Of interest, 12 h of refeeding after 5 h of starvation increased FAT-6:YFP levels higher than well-fed cohorts (Figure 2D), suggesting that when prolonged starvation occurs, a male's physiology can adapt to future food stress.

Day 2 adult males deprioritize feeding behavior and increase exploratory behavior

Since FAT-6:YFP expression levels decreased after acute food deprivation, we asked if the changes in the fluorescence in a well-fed day 2 wild-type male (Figure 1E) might be correlated with changes in feeding behavior. To assay feeding, we introduced well-fed day 1 and day 2 males to a lawn of *E. coli* expressing a red fluorescent protein and measured how fast ingested fluorescent bacteria accumulated in the intestine (Figure S3A). Surprisingly, we found bacterial consumption decreased as adult males aged from day 1 to day 2 (Figure 3A).

To determine if a day 2 wild-type male's decreased food ingestion also alters its mating behavior, we examined the male's food-seeking and copulation preferences. We designed a device to monitor a day 1 or day 2 male's choice to feed, mate, or explore its environment (see STAR Methods). The NGM agar

mating arena contained three paralyzed hermaphrodites (lying on no food), diagonally opposite a bacterial lawn (Figure S3B). After an hour, to allow hermaphrodite and bacterial secreted cues to permeate the arena, a single day 1 male (~12 h after L4 molt) or day 2 male (~36 h after L4 molt) was added to the arena and behavior was digitally recorded for 1 h. We plotted the proportion of time spent on mating (M), feeding (F), and exploring (E) on a ternary graph (Figure 3C), with each vertex representing one of the three behaviors. As a data point's distance from the vertex decreases, the proportion of time spent on that specific behavioral state increases. From our observations, day 2 males spent less time eating and more time exploring and mating than day 1 males (Figures 3C and S3C).

Previous research showed that hidden Markov models can be used in *C. elegans* hermaphrodites to analyze behavioral states, such as roaming, dwelling, and quiescence (Gallagher et al., 2013). Markov modeling explains behavior by assuming the transitions between behaviors follow defined probabilities. We wanted to see if similar modeling could explain the behavioral patterns and variabilities that we observed in the males (See methods). The behaviors collected across ~32 males resulted in a large dataset showing unique patterns of stochastic-like behavior, proving difficult to interpret (Figure 3B). Thus we used Markov modeling to describe behavioral transitions sequentially with fewer parameters while remaining stochastic.

We proceeded with a first order Markov model, which assumes a male's future behavior in 15 s is only affected by its current activity (Figures S4A and S4B). However, simulated behaviors from this model did not match the durations and distributions of the behaviors observed in live animals. On the other hand, simulations from a second order model (Figure 3D, the red dots), which further incorporates what the male was doing 15 s in the past, best matched the observed data.

The behavioral transition probabilities of the Markov model can be displayed as a state diagram or as a transition matrix (Figures 3E, S4C and S4D). We designed a state diagram to illustrate the male's choices for future behaviors based on its present (first order) and past behavioral states (second order). In our state diagram (Figure 3E), the sequence of the three behavioral states is displayed with possible transitions between exploring (yellow), feeding (blue), or mating (red). The age-specific proportion, the probability of transitioning to a specific future state based on its present and past state, is displayed adjacent to the state diagram (Figure 3E). For example, if a male was previously feeding and is currently exploring, the proportion of males expected to continue to explore would be 0.05 and would increase (green arrow) to 0.18 in day 2 males. From the model, we found day 2 males were biased toward a transition to exploration despite past behavioral choices (Figure 3E). In addition, transitions to feeding decrease despite past behavioral choices (Figure 3E). Interestingly, although older males appear to spend more time mating (Figure 3D), the modeling proportion values of the exploring-exploring-mating (EEM) suggest the male's mating drive between the two days are mostly unchanged (Figure 3E). Altogether, we suggest that wild-type male's reduced feeding behavior, coupled with its increased exploratory behavior, indirectly promotes the frequency and duration of a day 2 male's mating incidence.

We then asked if reduced Δ9 fatty acid desaturase function alters the male's feeding, mating, and exploring choices. We found, similar to wildtype (Figure 3D), the observed and modeled behavioral choices of *fat-6(lf); fat-7(lf)* males, showed increases in exploring from day 1 to day 2 (Figure 3F). Simulations from the Markov modeled proportions suggest that although day 2 mutant males appear to spend more time mating (Figure 3F), the mutants mating drive (EEM) between the two days is mostly unchanged (Figure 3G), similar to aging wild-type males (Figure 3E).

When we compared wild-type and *fat-6(lf); fat-7(lf)* males' behavioral choices (Figure 3B) and proportions (Figure 3I), we observed premature increases in exploratory behavior in the double mutant, supported by significant increases in recurrent exploring behavior (EEE) (Figure 3J). A comparison of proportions for day 2 wild-type and mutant males showed mutants had a lower probability of continued feeding given past exploring (EFF) (Figures 3I–3K). Differences in *fat-6(lf); fat-7(lf)* exploratory behavior are not unexpected, since the mutant's disrupted fat metabolism might mimic aspects of the metabolic state associated with starvation. Both food stress and food foraging have been correlated with sustaining exploratory behavior in hermaphrodites (Ben Arous et al., 2009; Calhoun et al., 2015; Gray et al., 2005; Hills et al., 2004; Pradhan et al., 2019; Sawin et al., 2000; Van Gilst et al., 2005). Altogether, reduced feeding in day 2 wild-type males might contribute for some of the changes in day 2 fat metabolism.
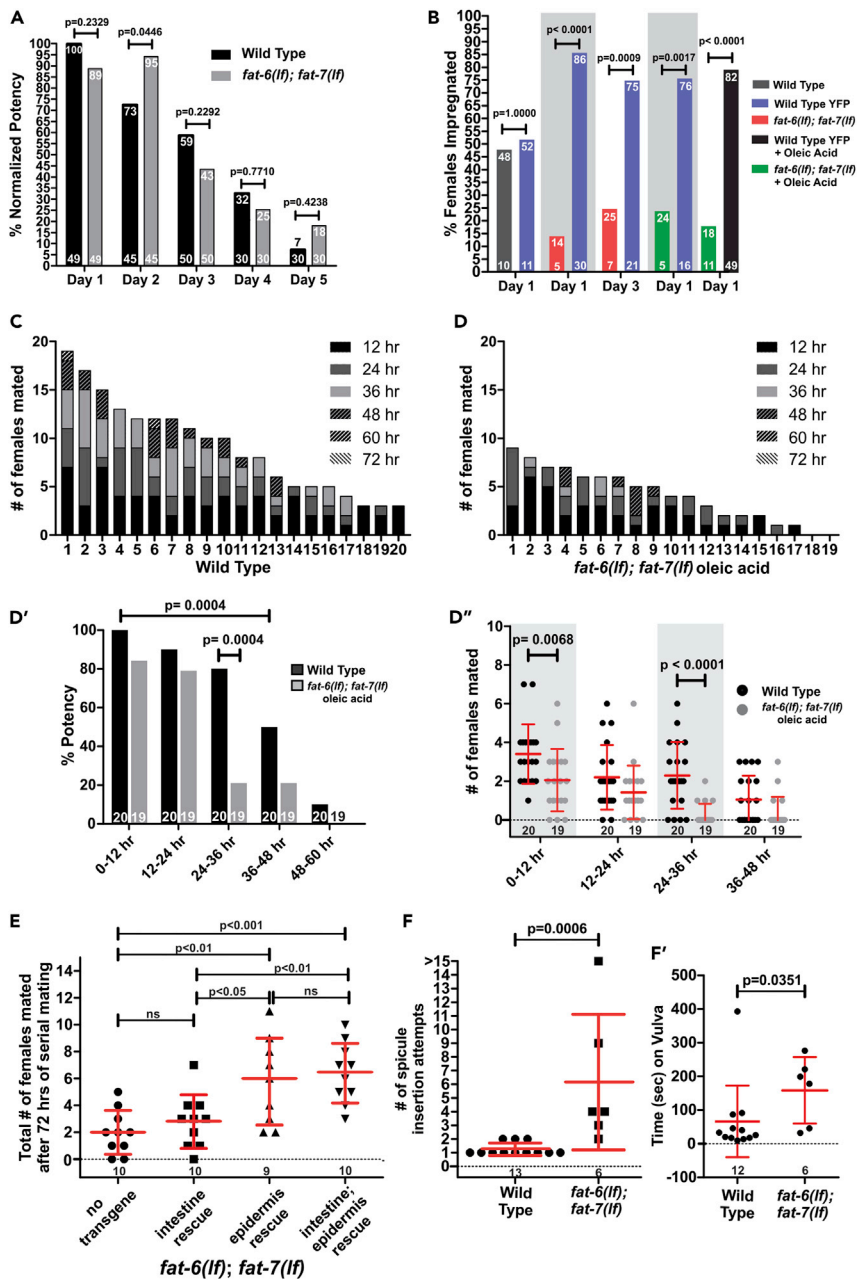
Figure 4. Mating performance and fitness of *fat-6*(*lf*); *fat-7*(*lf*)males

(A) The mating potency of wild-type and *fat-6*(*lf*); *fat-7*(*lf*) males. The percentages of successful matings are listed at the top of the bars. Numbers of animals assayed are listed at the bottom. p values were determined using Chi-square and Fisher exact test.

(B) The mating fitness of competing wild-type and *fat-6*(*lf*); *fat-7*(*lf*) males. Wild-type males carrying a fluorescent protein (*pck-2*:YFP) were competed against wild-type males lacking a fluorescent protein. Because both strains were found to be equivalent, wild-type males carrying a fluorescent protein were used in competition assays against *fat-6*(*lf*); *fat-7*(*lf*) males. The percentage of females mated is listed at the top of the bars. Numbers of animals assayed are listed at the bottom. p values were determined using Chi-square and Fisher exact test.

(C and D)The serial mating assay results of wild-type and *fat-6*(*lf*); *fat-7*(*lf*) males. The number of females impregnated is seen from 12 h, bottom black rectangle, to 72 h in rectangular subdivisions. Each column of rectangles represents a single male across 72 h. Males are organized, from left to right, by the total sum of females impregnated.

(D′ and D″) The percent of mated males and number of females impregnated, in the serial mating assays (C and D), across 72 h, was quantified and re-visualized in 12-h increments. Bars and whiskers represent mean and SD. p values for (D′) were determined using Chi-square and Fisher exact test. p values for (D″) were determined using unpaired t-test.

Figure 4. *Continued*

(E) Quantification of 72 h of serial copulation of intestinal and/or epidermal *fat-6* rescue in *fat-6(lf)*; *fat-7(lf)* males. Bars and whiskers represent mean and SD. p values were determined using one-way ANOVA with Bonferroni's multiple comparison posttest.

(F and F')Analysis of mating video recordings of *fat-6(lf)*; *fat-7(lf)* males. We quantified the number of spicule insertion attempts and the time on the vulva. Numbers of animals assayed are listed at the bottom. Bars and whiskers represent mean and SD. p values were determined using unpaired t-test.

Regulated fatty acid metabolism in the epidermis promotes mating fitness

The behavioral choice assay showed lipid metabolism disruption does not alter male reproductive drive between days 1 and 2; however, we did not know how copulation performance was affected. We used a potency assay to determine if the *fat-6(lf)*; *fat-7(lf)* mutations disrupted copulation performance. A single day 1-5 adult male is paired with a moving *pha-1(lf)* hermaphrodite, whose self-progeny dies at room temperatures. After a week of co-incubation, if the hermaphrodite produced at least one viable cross-progeny at room temperature, then the male is scored as potent. Surprisingly, during day 1-5 of adulthood, the kinetics of *fat-6(lf)*; *fat-7(lf)* males mating potency is similar to wild-type males; although day 2 mutant males were slightly more potent than wildtype (Figure 4A).

The wild-type-like decay profile of *fat-6(lf)*; *fat-7(lf)* mating potency is different from other previously studied mutants. For example, metabolic mutants of *sir-2.1*, a NAD-dependent deacetylase metabolic gene regulator, and *pck-2*,which encodes the gluco-/glyceroneogenesis enzyme PEPCK, declined in mating performance after day 1 (Goncalves et al., 2020; Guo and García, 2014). Because *fat-6(lf)*; *fat-7(lf)* copulation potency did not prematurely decline, we asked if mating fitness was affected. We assessed mating fitness by both the ability to out-compete other males for mates and to impregnate multiple mates. Mating fitness was first examined by competing a single wild-type and *fat-6(lf)*; *fat-7(lf)* male on a 5 mm bacterial lawn, containing a single moving *fog-2(lf)* female. The first male to impregnate the female within 3 h was deemed successful. To confirm paternity, the wild-type males and the cross-progeny, contained the PCK-2:YFP marker (Goncalves et al., 2020). In the control experiment, the YFP marker did not interfere with copulation (Figure 4B). When we addressed the fitness of day 1 and day 3 *fat-6(lf)*; *fat-7(lf)* males, we found that for both days, 75–85% of *fat-6(lf)*; *fat-7(lf)* mutants lost to wild-type males (Figure 4B), indicating they were competitively less fit.

One complication with the *fat-6(lf)*; *fat-7(lf)* mutants is their slowed development to adulthood; the limited production of unsaturated fat likely delays growth and alters cell lipid membrane composition. To address whether failure to produce unsaturated lipids indirectly affects behavioral fitness, we uncoupled unsaturated lipid storage from saturated lipid catabolism by feeding *fat-6(lf)*; *fat-7(lf)* males oleic acid; the supplemented mono-unsaturated lipids will rescued lipid storage, but the mutants should still not metabolize the bacterially ingested lipids properly (Brock et al., 2006, 2007). We observed that oleic acid-fed males' copulation fitness were still uncompetitive against wildtype and oleic acid-fed wildtype (Figure 4B), indicating that despite mating competency under non-competitive conditions, dysregulated lipid catabolism reduces mating fitness.

Because *fat-6(lf)*; *fat-7(lf)* males could not outcompete wild-type males, we asked if disrupting fat metabolism also alters the male's fitness to impregnate multiple mates over time. To assay the mating endurance of aging males, a single 12-h adult (day 1) wild-type, *fat-6(lf)* single mutant, *fat-7(lf)* single mutant or oleic acid-fed *fat-6(lf)*; *fat-7(lf)* double mutant male was placed with ten day 1 virgin *fog-2(lf)* females on a 5 mm diameter bacterial lawn. Every 12 h, impregnated females were counted, removed, and replaced with similarly aged virgin females; additionally, the male and virgin females were moved to a fresh lawn (Goncalves et al., 2020). After quantifying 72 h of serial mating fitness, wild-type males mated with 4–18 females, with a mean of nine females per male (Figures 4C and 4D''). Furthermore, wild-type males were able to perform copulation without decline up to 36 h of adulthood (Figure 4D'). The mating fitness and potency assay (Figure 4A) differ in that the serially mating males are not virgins after their first copulation, while potency is determined with an aged virgin male and is contingent upon incubation with a single mate for unconstrained time. In regards to *fat-6(lf)* or *fat-7(lf)* single mutants, their mating profiles were not substantially different from wildtype (Figures S5A and S5B), confirming that the Δ9 fatty acid desaturase genes can compensate mutually. Contrary to wildtype and single mutants, oleic acid-fed *fat-6(lf)*; *fat-7(lf)* males decreased in mating performance after 24 h (Figures 4D and 4D'). As for mating fitness, the double

mutants significantly mated with fewer females between 0-12 h and 24–36 h (Figure 4D''). The period of time between 24 and 36 h is noteworthy, as it precedes the *fat-6* RNA increases seen in wild-type males from 36-48 h. These observations suggest *fat-6* expression in one or more tissues maintains serial mating robustness.

To address where *fat-6* functions for copulation, we expressed *fat-6*:YFP in the *fat-6*(*lf*); *fat-7*(*lf*) male intestine (using the *gtl-1* promoter) (Figure S5C) and/or epidermis (using the *dpy-7* promoter) (Figure S5D) (Johnstone and Barry, 1996; Teramoto et al., 2005). We then asked if transgenic *fat-6* expression increases the number of serial impregnations after 72 h of mating. Intestinal FAT-6:YFP did not improve the total number of impregnations (Figures 4E and S5E) despite restoring fixative Nile Red-stained lipid stores (Figure S5F). Surprisingly, epidermal *fat-6*:YFP expression also rescued intestinal Nile Red-stained lipid stores, suggesting that mono-unsaturated lipids formed in the epidermis can mobilize to other tissues (Figure S5F).Additionally, mutant males expressing epidermal FAT-6:YFP mated with more females during the first 72 h of adulthood (Figures 4E and S5E). *fat-6*(*lf*); *fat-7*(*lf*) males' mating endurance also improved with the expression of FAT-6:YFP in both intestine and epidermis; however, not significantly better than the epidermal expression alone (Figures 4E and S5E). The tissue specificity for *fat-6* expression to enhance the behavior of day 2 mutants suggest that neurons and muscles involved with copulation are more reliant on the lipid formation, utilization and/or mobilization from the epidermis than the intestine.

Finally, we asked which mating-based motor steps are affected by reducing Δ9 fatty acid desaturases. We recorded the mating attempts of day 1 wild-type and *fat-6*(*lf*); *fat-7*(*lf*) males with locomotion defective and easy to penetrate hermaphrodites. Within a 10-min observation window, we noted that wild-type males inserted their copulatory spicules immediately into hermaphrodites within one or two attempts of contacting the vulva (Figure 4F). In contrast, double mutant males had difficulty in maintaining their position over the vulval slit, despite recognizing the hermaphrodites' vulva and inducing repetitive high frequency spicule thrusts. The double mutant males would slip off the vulva and then reattempt spicule insertion between 2 and >15 times before insertion and ejaculation (Figure 4F). This defect increased the time double mutant males spent attempting to breach the vulva (Figure 4F'). Because spicule intromission requires males to maintain a stable position over the vulva while contracting their protractor muscles, the double mutant's deficit could be indicative of a defect in cholinergic motor control of muscles involved in both body posture and spicule motion (Gao et al., 2018; Gao and Zhen, 2011; Kawano et al., 2011; Liu et al., 2011; Wen et al., 2012).

Cholinergic secretion and neural activity are increased in stearoyl-CoA desaturase deficient males

Since *fat-6*(*lf*); *fat-7*(*lf*) males showed difficulty with spicule insertion during mating, we asked if the cholinergic stimulation of the spicule protractor muscles was defective. To address this, we exposed wild-type and *fat-6*(*lf*); *fat-7*(*lf*) males to increasing concentrations of arecoline. Arecoline is a non-specific acetylcholine receptor (AChR) agonist that induces neuromuscular depolarization in the male tail, resulting in spicule protraction (Correa et al., 2012). We found the double mutant's response to exogenously applied arecoline was similar to wild-type (Figure 5A). This suggests that activation of AChRs, either in neurons or muscles, results in functional tonic spicule muscle contraction.

To address the possibility of altered cholinergic neuron activity, we asked if cholinergic secretion from the SPC, PCB, or PCC sensory-motor neurons was different in the double mutant. These neurons synapse directly with the protractor muscles, which when contracted results in spicule protraction from the cloaca. To address this, we used the drug aldicarb which inhibits acetylcholine (ACh) esterase, an enzyme responsible for degrading acetylcholine at the synaptic cleft (Miller et al., 1996; Nguyen et al., 1995; Rand and Russell, 1985). When ACh esterase is inhibited, ACh buildup from spontaneous release results in sex muscle contraction and spicule protraction; reduced ACh transmission will delay aldicarb-induced spicule protraction, whereas enhanced ACh transmission will hasten spicule protraction (Garcia et al., 2001). We placed wild-type and mutant males on NGM agar pads infused with 5, 10 or 15 mM aldicarb and measured how fast exposure to the drug causes the males to protract their spicules. On 5 and 10 mM aldicarb, males were unresponsive to the drug during the observation period. However, at 15 mM aldicarb, *fat-6*(*lf*); *fat-7*(*lf*) males protracted their spicules faster than wild-type (Figure 5B). This observation suggests that a deficiency in Δ9 fatty acid desaturases might increase spontaneous cholinergic release in the spicule protraction circuitry.
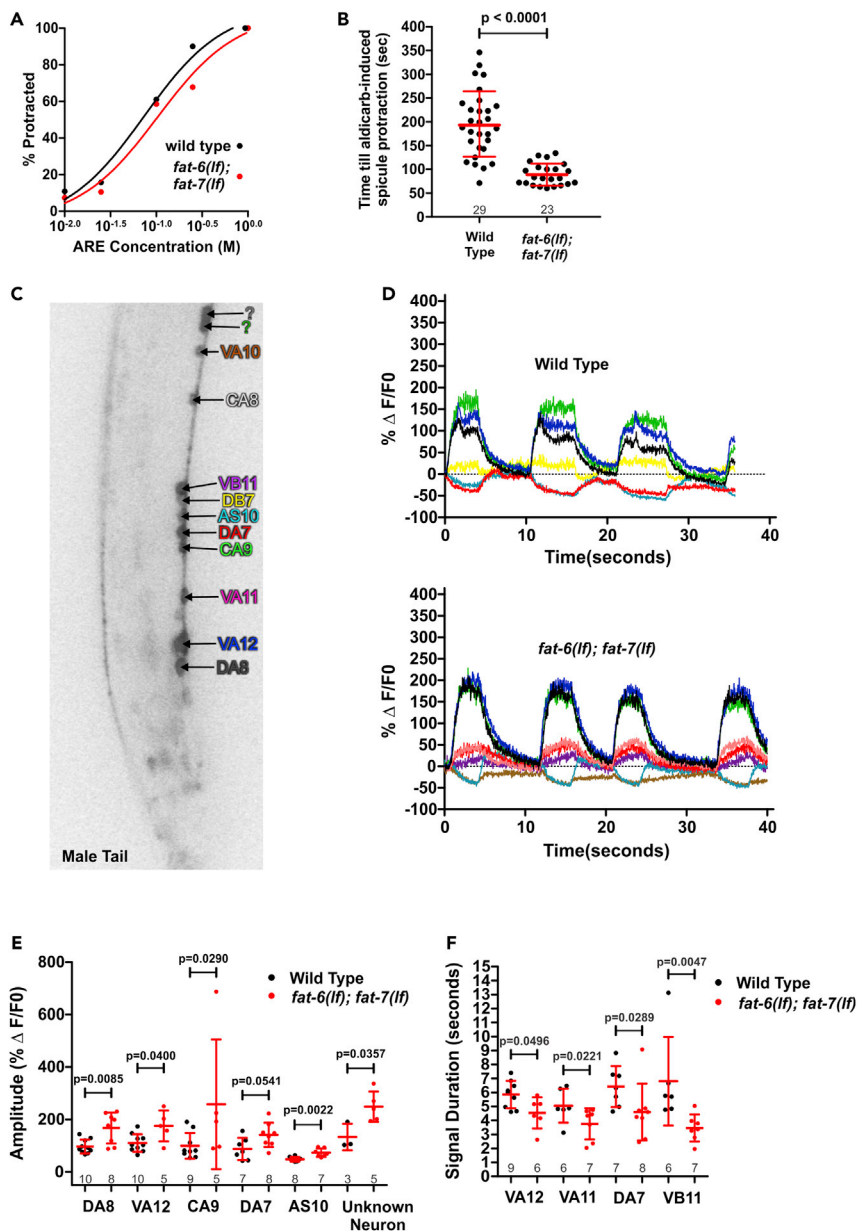
Figure 5. Characterization of cholinergic neurons in *fat-6(lf); fat-7(lf)*males

(A) Day 1 wild-type and *fat-6(lf); fat-7(lf)* males show similar response to the AChR agonist arecoline (ARE).

(B) Wild-type and *fat-6(lf); fat-7(lf)* day 1 males were placed on NGM pads infused with 15 mM aldicarb. We quantified the time until protraction of the spicule, which is a proxy for muscle contraction. Bars and whiskers represent mean and SD. p values were determined using unpaired t-test.

(C) G-CaMP6 calcium sensor fluorescence was digitally recorded in wild-type and *fat-6(lf); fat-7(lf)* day 1 males mounted on 10% noble agar containing Polybead polystyrene 0.1 μm microspheres. Ellipse-shaped ROIs were drawn for 12 cholinergic neurons.

(D) Example of cholinergic Ca^{2+}-induced fluorescence changes in a wild-type and a *fat-6(lf); fat-7(lf)* male. Fluorescence waves, color-coded to their respected neurons, were plotted across time. The colors of the lines match the colored neuron names in (C).

(E) Amplitude of neuronal calcium waves, measured as the average difference between the local min and max of waves.

(F) Signal duration of neuronal calcium waves, measured as the average duration of fluorescence above the threshold, which is set by taking the mean fluorescence of the neuron. For (E) and (F), each dot represent one neuron recording of one male, bars and whiskers represent mean and SD. p values were determined using unpaired t-test.

We expect that spicule intromission requires appropriate cholinergic motor control of muscles involved in both body posture and spicule motion. The cholinergic motor control of muscles involved in body posture is regulated by motor neurons indirectly connected to the protraction circuitry. Thus, we asked if cholinergic motor neurons in the male posterior ventral cord might also have heightened activity (Brittin et al., 2021; Cook et al., 2019; Jarrell et al., 2012; Sulston, 1976; Sulston et al., 1980, 1983; Sulston and Horvitz, 1977). We used the promoter of a vesicular acetylcholine transporter *unc-17* to drive the expression of the G-CaMP6 fluorescent calcium sensor in these neurons (Figure 5C) (Alfonso et al., 1993, 1994a, 1994b; Chen et al., 2013). Because recording these neurons' activity during copulation is challenging, we restrained wild-type and *fat-6*(*lf*); *fat-7*(*lf*) males under a coverslip using 10% noble agar and Polybead polystyrene 0.1 μm microspheres (Kim et al., 2013). As the males struggled under the coverslip, we were able to record changes in the neuronal calcium transients.

From the digital recordings, ROIs were drawn over individual neurons and calcium responses were measured for ~40 s (Figures 5D and S6A). The double mutants showed higher calcium transients in the posterior cholinergic ventral cord neurons DA8, VA12, CA9, DA7, AS10, and a neuron we could not conclusively identify (Figure 5E); the other neurons, VA11, DB7, VB11, CA8, VA10, and an additional ventral cord neuron we could not conclusively identify, produced average calcium transients similar to wildtype (Figure S7A). In addition, for some neurons in the double mutant, such as VA12, VA11, DA7, and VB11, the average signal duration was also shorter (Figure 5F), suggesting faster repolarization; the other neurons, DA8, CA9, AS10, DB7, CA8, VA10, and two additional ventral cord neuron we could not conclusively identify, produced average signal duration similar to wildtype (Figure S7B). These observations suggest that in males lacking Δ9 fatty acid desaturases, defects in lipid metabolism can exaggerate the intensity and shorten the duration of cholinergic neural activity in some of the cells.

Stearoyl-CoA desaturase deficiency alters ERG-like/UNC-103 K$^+$ channel expression levels

The increased spontaneous ACh release and altered calcium transients suggest the regulation of neuronal membrane threshold and repolarization are perturbed. These processes are partially regulated by K$^+$ channel activity (Alqadah et al., 2016; Collins and Koelle, 2013; Liu et al., 2007, 2014; Steciuk et al., 2014; Wang et al., 2001). Previous research has identified ERG (*ether-a-go-go-related gene*)-like/UNC-103, EAG (*ether-a-go-go*)/EGL-2, and BK (*big potassium*)/SLO-1 K$^+$ channels participate in regulating the excitability of the spicule protraction circuit. Defects in these channels will induce spontaneous sex muscles contraction, causing the spicules to protract out of the tail; this phenotype is referred to as Protraction constitutive, Prc. However, in the absence of any one of these K$^+$ channels, a compensatory upregulation of the remaining K$^+$ channels can ameliorate spicule protraction defects, reducing the probability of sex muscle spasms (LeBoeuf and Garcia, 2012). Of interest, food-deprivation stress, which leads to mobilization and catabolism of internal lipid stores, can further boost the compensatory increase in K$^+$ channel expression (Gruninger et al., 2006, 2008; LeBoeuf et al., 2007, 2011). Thus, we asked if *fat-6/7* deficiency affects K$^+$ channel expression.

To address this question, we performed RT-qPCR analysis of ERG-like/*unc-103*, EAG/*egl-2*, and BK/*slo-1* K$^+$ channels on day 1 wild-type and *fat-6*(*lf*); *fat-7*(*lf*) males. We used primers to the isoforms-shared exons in each of the genes to capture total expression of all isoforms. We generated single worm cDNA libraries, but decided to combine three worms' cDNA for each biological replicate to enhance the sensitivity. Only *unc-103* channel expression was found to be significantly down-regulated (Figure 6A). This result was surprising since *fat-6*(*lf*); *fat-7*(*lf*) males do not display the abnormal Prc phenotype like the *unc-103*(*lf*) males (Figure 6B).

unc-103 is broadly expressed in neurons and muscles, thus we used primers unique to ten *unc-103* isoforms to determine which tissue-specific isoforms were down-regulated (Reiner et al., 2006). We found all but two isoforms were below detection threshold in the double mutant; surprisingly, the two isoforms detected, *unc-103*A and D isoforms, were both upregulated (Figures 6C and 6C'). Likely, these two isoforms account for most of the *unc-103* signal for *fat-6*(*lf*); *fat-7*(*lf*) males in the previous RT-qPCR assay (Figure 6A). Isoform A is expressed in all body wall, intestinal muscle, sex muscles, and four neurons in the head. Isoform D is expressed in neurons URA, PVM, and one neuron in each of the male's nine pairs of copulatory sensory rays. The down-regulation of neuronal *unc-103* isoforms, B/C/E/F, could account for the heightened neural excitation and transmitter release whereas the upregulation of the muscle-expressed isoform A could mitigate
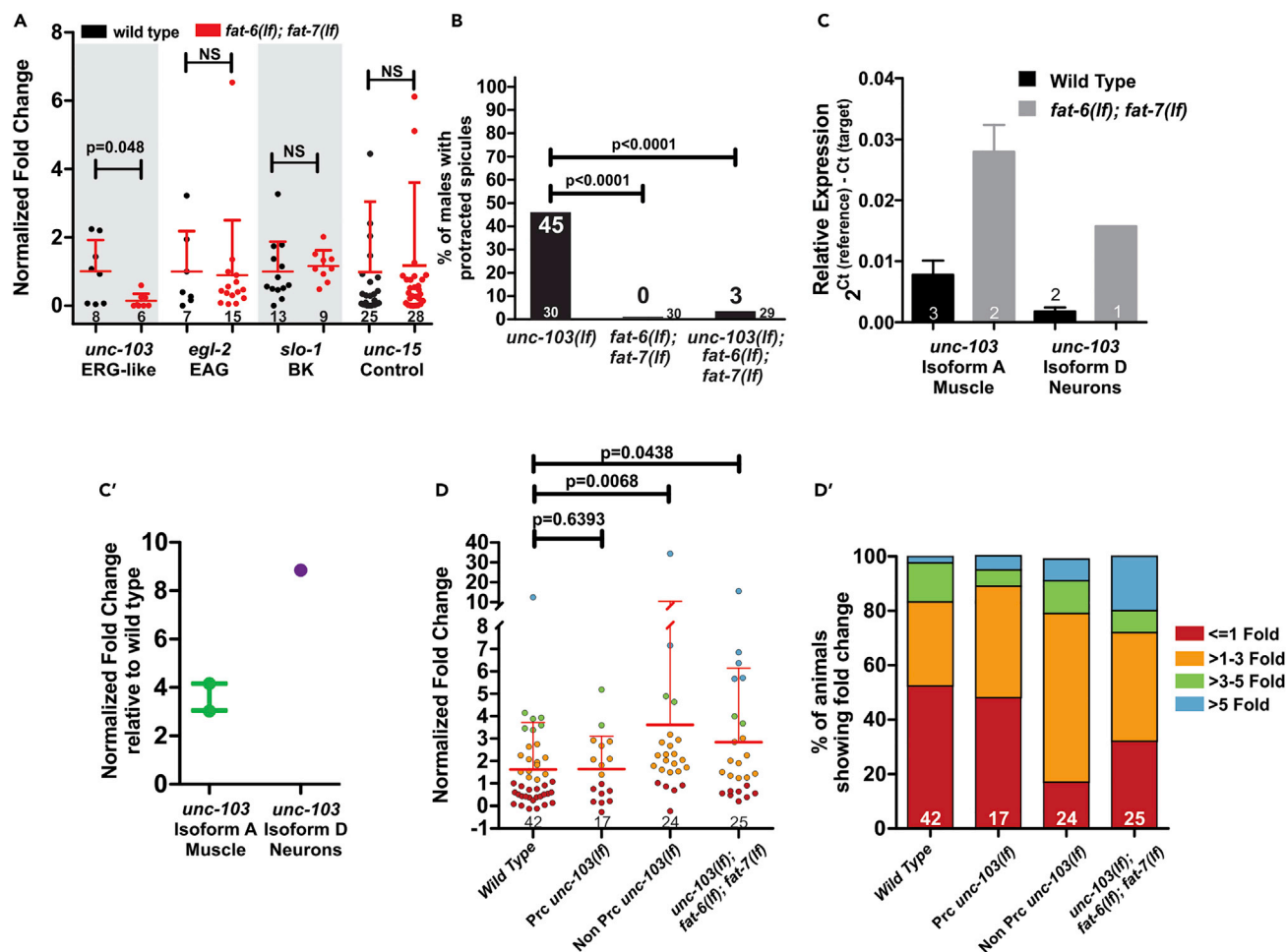
Figure 6. Dysregulated *unc-103* in *fat-6(lf); fat-7(lf)* males

(A) RT-qPCR results of ERG-like/UNC-103, EAG/EGL-2, and BK/SLO-1 K⁺ channels in wild-type and *fat-6(lf); fat-7(lf)* males (3 males/replicate). The result of the *unc-15* reference gene is also shown. Bars and whiskers represent mean and SD. p values were determined using the Mann Whitney non-parametric test.

(B) The percent of males displaying protracted spicules. L4 males were transferred to new plates and kept in groups of 15. Spicule protraction was quantified 12–15 h after transfer. p value was determined using a Chi-square and Fisher exact test. Values at the bottom of the bars denote number of males assayed. Values above the data denotes % spicule protracted.

(C) Single-worm RT-qPCR results of *unc-103* isoforms in wild-type and *fat-6(lf); fat-7(lf)* males. Attempts were made to measure all isoforms of ERG-like/UNC-103 K⁺ channels, but we could not reach comparable levels of all isoforms except isoform A/D in mutants. Bars and whiskers represent mean and SD.

(C')Data in C displayed as fold change normalized to wild-type *unc-103* isoform A and D.

(D) Single-worm RT-qPCR results of the EAG K⁺ channel gene *egl-2. unc-103* mutant males were separated based on spicule protraction phenotypes (Prc/NonPrc).Data was normalized to the median of the wild-type dataset. Bars and whiskers represent mean and SD. p values were determined using an unpaired t-test.

(D') Partitioning by fold change, based on (D), shows the major contribution to the mean. Triple mutant*egl-2* levels are biased to larger fold changes (>5-fold) versus Non-Prc *unc-103(lf)* (1.0-3.0). No p value was provided as this panel serves only as a different visual representation of data seen in (D). For (A)-(D') Values below the data denote the number of biological replicates.

possible downstream muscle spasms from the altered neural activity. However, we note that the RT-qPCR experiments measured in whole worms were performed using a limited number of primer sets. In addition, increased expression of K⁺ channels mRNA may not result in more channel protein expression or channel activity. Nonetheless, previous published papers have observed behavioral changes that occur with K⁺ expression in fed and starved aging wild-type males (Gruninger et al., 2006, 2008; LeBoeuf and Garcia, 2012; LeBoeuf et al., 2007, 2011).

We next asked whether UNC-103 K⁺ channels are involved in muscle function in the absence of Δ9 fatty acid desaturases. To address this, we created a triple mutant *unc-103(lf); fat-6(lf); fat-7(lf)* and asked if the Prc

phenotype is enhanced or suppressed. Surprisingly, *unc-103*(*lf*)*; fat-6*(*lf*)*; fat-7*(*lf*) males were suppressed for the *unc-103*(*lf*)-induced Prc phenotype (Figure 6B). This result prompted us to consider earlier work indicating that transient starvation, which results in increased TAG lipolysis, can increase EAG/*egl-2* K$^+$ channel gene expression. Thus, we asked whether *fat-6*(*lf*)*; fat-7*(*lf*) mutants, which are deficient in forming lipid stores, affect EAG/*egl-2* transcript expression. A quadruple *unc-103*(*lf*)*; egl-2*(*lf*)*; fat-6*(*lf*)*; fat-7*(*lf*) mutant was too sick to generate and maintain, so we performed single worm RT-qPCR analysis of *egl-2* on *unc-103*(*lf*)*; fat-6*(*lf*)*; fat-7*(*lf*) males; 0/25 showed the Prc phenotype (Figure 6D). We compared the triple mutants *egl-2*'s expression against wild-type and *unc-103*(*lf*) single mutant animals; additionally, we separated *unc-103*(*lf*) males displaying a Prc phenotype (17/41 males) or a non-Prc phenotype (24/41 males) (Figure 6D). We found that for Prc-displaying *unc-103*(*lf*)mutant males, *egl-2* expression levels were not significantly different from wild-type males (Figure 6D). However, for both the sub-population of non-Prc *unc-103*(*lf*) single mutant males and the *unc-103*(*lf*)*; fat-6*(*lf*)*; fat-7*(*lf*) triple mutants, *egl-2* expression was significantly elevated (Figure 6D). When we analyzed the distribution of *egl-2* expression, a significant proportion of triple mutant males showed greater than 5-fold increases in *egl-2*,which differed from the response of other assayed males (Figure 6D'). Altogether, we suggest decreased lipid storage and/or increased lipid oxidation can alter K$^+$ channel RNA expression.

DISCUSSION

Previous work has established the role of enhanced glycolytic and fatty acid oxidation processes in behavioral decline (Guo and García, 2014). Despite the detrimental effects of oxidative metabolism with age, behavioral performance is similar across days 1-2 of adulthood in males. We postulate that metabolic adaptations are present to counteract changing catabolism. For hermaphrodites, age dependent metabolic shifts have been seen in the expression patterns of insulin signaling genes *ins-7*, *ins-19*, *ins-13/acdh-2*, *ins-29* and *ins-37* (Baugh et al., 2011). Here, we found the metabolic gene expression of stearoyl-CoA desaturases (SCD) increased on day 2 of adulthood in males. SCDs, encoded by *fat-5*, *fat-6*, and *fat-7*, catalyze the rate limiting step of monounsaturated fatty acid synthesis (Watts and Browse, 2000). Our results showed that epidermal *fat-6* was sufficient to establish intestinal lipid storage and required to maintain mating fitness with age (Figures S5F and 4E).

The epidermis is a multinucleated tissue that can store lipids (Figure 7A). In the epidermis of larva undergoing starvation, regulated lipolysis is mediated by epidermal AMP-activated protein kinase signaling and adipose triacylglyceride lipases (Narbonne and Roy, 2009). In addition, trehalose, which can be created and catabolized into glucose in the epidermis, has been shown to act as a fuel source to support larval starvation-dependent increases in lifespan (Hibshman et al., 2017). In this work, we suggest that epidermal *fat-6* is required for regulated lipid droplet lipolysis during day 2, to provide the neighboring neuromuscular circuitry with lipid-derived acetyl-CoA (Figures 7B and 7C). Cross-talk between the epidermis and neurons has been previously explored through elimination of cholinergic excitatory synapses and disruption of NAD$^+$ synthesis during axon regeneration (Cherra et al., 2020; Cherra and Jin, 2016; Kim et al., 2018). We speculate that day 2 adult males, which have moderated their feeding behavior, retain the regulation that occurs in the larval epidermis to maintain epidermal lipid stores for neuromuscular function.

Our analysis of the FAT-6:YFP knock-in showed that in aging wild-type *C. elegans* males, the degradation of FAT-6 stearoyl-CoA desaturases was spatially regulated throughout the intestine (Figures 1D and 1E). We hypothesize that the continuous expression of FAT-6 in the anterior intestine facilitates absorption and conversion of dietary fats into lipid storage (Figures 1F and 1G). The posterior intestine expression likely provides unsaturated fats for reproductive processes such as sperm and seminal fluid production. This was supported through gonad ablation (Figure S2F) and also builds on known NHR-80-dependent increases of intestinal *fat-6* in germline-depleted mutants (Goudeau et al., 2011).

We observed increases in *fat-6* transcription between days 1 and 2 of adulthood in wild-type males (Figure 1A). We expect that changes in lipid metabolism gene expression might correlate with decreases in feeding behavior (Figure 3A). Studies from others have shown that during fasting, sterol levels decrease and a family of transcription factors, called sterol regulatory-element binding proteins, are induced to elevate lipid synthesis genes (Goldstein et al., 2006; Nomura et al., 2010). Surprisingly, we observed that FAT-6 protein levels decreased in the intestine on day 2, despite the increase in mRNA levels (Figures 1D and 1E). We expect that changes in feeding behavior might trigger mTOR inhibition and
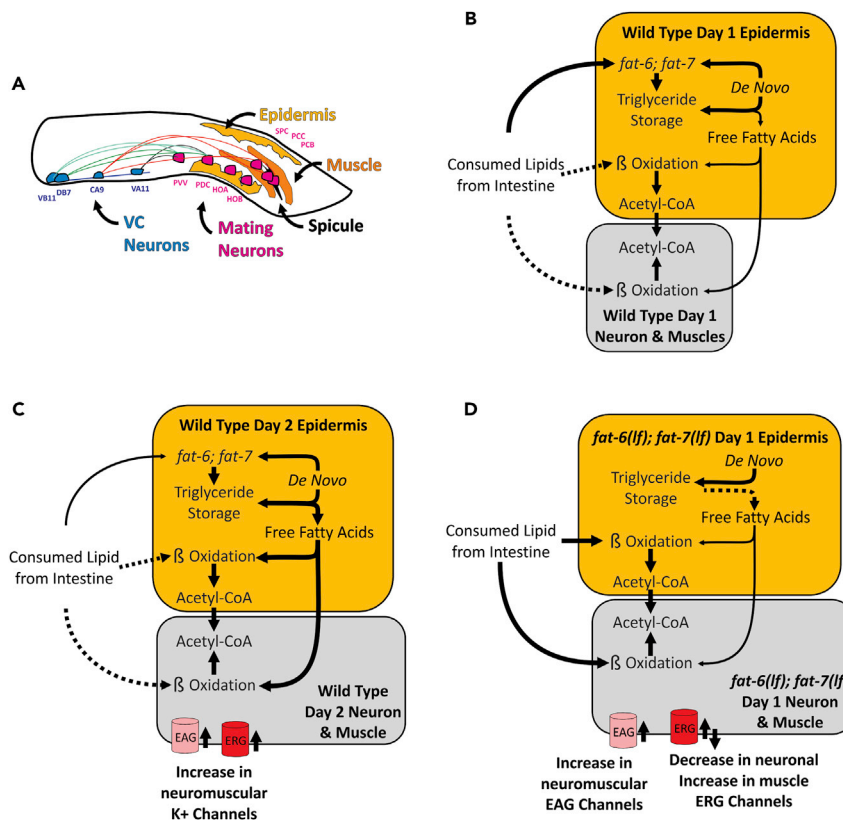
Figure 7. FAT-6/7 maintains lipid droplets as day 2 adult male lipid oxidation occurs

(A) Tissues required for mating behavior are colorized with a yellow epidermis, orange muscles, pink neurons used for vulva sensing and spicule insertion, and blue ventral cord neurons used for the control of locomotion and male tail stability. The ventral cord neurons are connected either through gap junctions or synapses to neurons involved in spicule insertion. For example, VB11, DB7 and VA11 are connected to the PDB, PDC, or PVV neurons controlling copulatory locomotion and posture after sensing the vulva through HOA or HOB. PVV neurons in turn also connect either through synapses or gap junctions to PCB controlling appropriate sensing of the vulva and spicule insertion. Male specific CA9 is indirectly connected either by gap junctions or synapses to the spicule insertion cholinergic neurons SPC, PCB, and PCC (Brittin et al., 2021; Cook et al., 2019; Jarrell et al., 2012; Sulston, 1976; Sulston et al., 1980, 1983; Sulston and Horvitz, 1977).

(B) A summary of expected lipid metabolism in day 1 adult males. Dotted arrows represent pathways not expected or unlikely to occur. Thicker arrows indicate prioritized lipid metabolism. The golden and gray box represents the conditions in epidermal and neuromuscular tissues, respectively. Day 1 males consume dietary lipids and prioritize the synthesis of lipid storage in the epidermis. Consumed lipids from the intestine are not oxidized under *ad libitum* conditions. Lipolysis and β-oxidation persist to maintain homeostasis. Metabolic byproducts can be used in fat synthesis, *de novo*, to form lipid storage.

(C) A summary of expected lipid metabolism in day 2 adult males. Dotted arrows represent pathways not expected or unlikely to occur. Thicker arrows indicate prioritized lipid metabolism. The golden and gray box represents the conditions in epidermal and neuromuscular tissues, respectively. Despite *ad libitum* conditions, day 2 adult males decrease feeding behavior. As dietary fat ingestion decreases, lipolysis of lipid stores is prioritized. Under these conditions, fatty acid desaturases play a role in maintaining lipid droplet stores as the oxidation of lipid droplets becomes a source of metabolic fuel.

(D) A summary of expected lipid metabolism in day 1 adult *fat6(lf); fat-7(lf)* mutant males. Dotted arrows represent pathways not expected or unlikely to occur. Thicker arrows indicate prioritized lipid metabolism. The golden and gray box represents the conditions in epidermal and neuromuscular tissues, respectively. Under *ad libitum* conditions, the inability to create lipid storage results in dietary fat ingestion and immediate oxidation. To compensate for increased *fat-6(lf); fat-7(lf)* lipid oxidation, muscle ERG-like/UNC-103 and EAG/EGL-2 channels are upregulated, resulting in the modulation of muscle excitation involved in posture and spicule movement. In the circumstance of *fat-6; fat-7* deficiency, calcium activity of motor neurons increase with dysfunctional lipid catabolism on day 1.

ubiquitin-proteasome system (UPS) leading to increased FAT-6 turn-over (Huang and Manning, 2008; Kato et al., 2006; Menon et al., 2014; Zhao et al., 2015). Given the need for epidermal FAT-6 to rescue *fat-6*(*lf*); *fat-7*(*lf*) mating behavior (Figure 4E), we suggest a basal production of FAT-6 results in sufficient lipid storage formation.

Despite the upregulation of *fat-5* in a *fat-6*(*lf*); *fat-7*(*lf*) mutant, the low-fat phenotype persists (Figures 2A and 2D). Contrary to this finding, previous work showed that a *daf-2*(*lf*); *fat-6*(*lf*); *fat-7*(*lf*) hermaphrodite has an altered 16:1 to 16:0 lipid ratio and increased fat stores; thus under certain circumstances, *fat-5* can better compensate for *fat-6/7* deficiency (Dickinson et al., 2013). This is likely through the function of *daf-16*, which when additionally mutated, restored the *daf-2*(*lf*); *fat-6*(*lf*); *fat-7*(*lf*) mutants to the low fat phenotype (Perez and Van Gilst, 2008). We expect that the copulatory deficiency of *fat-6*(*lf*); *fat-7*(*lf*) males is also due to suboptimal compensatory mechanisms (Figure 2D). Feeding behavior may be a mediator of metabolic gene expression in *fat-6*(*lf*); *fat-7*(*lf*) mutants, as activation of *daf-16* and specific NHRs can be induced by fasting (Hyun et al., 2016). Despite this, day 2 *fat-6*(*lf*); *fat-7*(*lf*) males, which exhibit decreased feeding, do not improve in copulation performance or fitness (Figure 4D). This observation suggests that a critical fasting period before adulthood may trigger appropriate compensation. This idea is supported by past work showing that L4 males undergoing food-deprivation can increase the expression of EAG (*ether-a-go-go*)/EGL-2 K$^+$ channels in the neuromuscular circuitry, resulting in prolonging mating behavior during aging (Gruninger et al., 2006, 2008; LeBoeuf et al., 2007, 2011).

The circuit responsible for spicule insertion during mating is composed of multiple sensory-motor neurons. The neurons control muscles capable of fast and slow twitch-like contractions. Upon contacting the vulva, cloacal sensory-motor neurons stimulate sex-common and sex-specific muscles to promote repetitive high frequency shallow spicule thrusts. When the spicules partially penetrate the vulval slit, the SPC proprioceptive motor neurons induce sustained spicule muscle contraction, which forces the spicules through the vulva. The different contractile behaviors of the spicule protractor muscles suggest a high energy demand, which may require epidermal lipolysis. The altered neuronal calcium transients in *fat-6*(*lf*); *fat-7*(*lf*) males (Figures 5E and 5F) and altered ERG-like/UNC-103 and EAG/EGL-2 channel mRNA transcripts (Figures 6C and 6D'), expressed in both muscles and neurons in the copulation circuits, suggest that epidermal lipid metabolism might regulate the cell excitability of circuit components involved in mating (Figures 7B–7D). In the absence of epidermal *fat-6* and *fat-7*-expressed stearoyl-CoA desaturase activity, there might be a deficiency of lipid-base fuel that is provided by the epidermis to the surrounding excitable cells.

Maintaining the appropriate excitable cell activity during mating requires energy demanding regulation of ions. We hypothesize a substantial metabolic requirement for the intromission circuitry to respond to the vulva and maintain extended sessions of mating. Also, the precise temporal regulation of motor programs likely requires external metabolic support. While this support may be heavily glucose dependent on day 1 of adulthood, since glucose partially rescues mating robustness in day 1 gluco-glyceroneogenesis deficient mutants (Goncalves et al., 2020), we also suggest a requirement of epidermal saturated and unsaturated lipids. A constant lipid supply might help maintain membrane potential thresholds used in triggering rapid on-and-off motor responses during extended stretches of copulation.

Alternatively, without epidermal *fat-6* and *fat-7* to promote lipid storage, there might also be chronic free fatty acids that can deleterious affect the physiology of muscles and neurons. Unregulated fatty acid oxidation or mitochondrial proton leak could result in reduction in ATP production and ROS-induced disruption of K$^+$ channel function. Previous work has shown increased lipid oxidation and radical production, such as hydrogen peroxide, alters the conformation of K$^+$ channels causing hyperpolarization (Jabr and Cole, 1993). The alterations in *unc-103* transcripts might indicate that the physiology of excitable cells involved in male copulation are remodeled to compensate for changes in lipid metabolism. We found that excitation of *fat-6*(*lf*); *fat-7*(*lf*) mutant musculature might be modified due to changes in expression of ERG-like/ UNC-103 K$^+$ channels (Figures 6C and 7D). The expression of *unc-103* deviates in an isoform specific manner, which we expect results in unique changes across various excitable cells. For example, we postulate that decreased neuronal *unc-103* could account for increased neuronal activity, which can be offset by increased muscular *unc-103* expression.

Previously published work has shown that neurons secrete fatty acids, which then undergo lipolysis in astrocytes, to avoid activity dependent dysfunction (Ioannou et al., 2019). The authors induced neuronal

excitotoxicity and measured increases in lipid peroxidation and neuronal lipoprotein fatty acid mobilization to astrocytes (Ioannou et al., 2019). Although we did not observe neuronal death in day 1-2 wild-type and day 1 *fat-6*(*lf*); *fat-7*(*lf*) males, we expect that increased cell excitability with age, previously shown in *C. elegans* males (Guo et al., 2012), could be exacerbated or caused by increased fat catabolism. Hence, we suggest that the epidermis is a potential mediator of increased neuronal lipid metabolism on and after day 1 of adulthood (Figures 4E, 7A and 7B). In addition, excitotoxicity is thought to be caused by over-activation of glutamate receptors resulting in inward currents of Na^+ and Ca^{2+} (Dong et al., 2009). In turn, proteases are activated by calcium and damage a variety of proteins involved in cytoskeleton and metabolism (Dong et al., 2009). The calcium transients observed in *fat-6*(*lf*); *fat-7*(*lf*) suggest an exaggerated calcium inward current (Figure 5E). Of interest, the calcium currents, in *fat-6*(*lf*); *fat-7*(*lf*) males, were extinguished quicker than those seen in wild-type males (Figure 5F). We suggest that changes in EAG/EGL-2 K^+ channel expression may play a role in repolarizing neurons, involved in posture and spicule movement, in *fat-6*(*lf*); *fat-7*(*lf*) (Figures 6D and 7D).

The most obvious behavioral consequence of fat metabolism disruption on the neuromuscular circuits was reduced copulatory competitiveness and serial reproductive potency (Figures 4B and 4D). The *fat-6*(*lf*); *fat-7*(*lf*)-induced altered-lipid catabolism and reduced storage (Figure 7D) possibly interfere with motor processes tuned to glycolytic-mediated fuel. Recent work has shown that the enzyme PEPCK, which promotes gluco-glyceroneogenesis, can function in the epidermis to rescue mating behavior defects (Goncalves et al., 2020).While intestinal *fat-6* expression rescues developmental and morphological defects, specific tissues may require a constant supply of specialized metabolites. For example, glucose partially rescues mating robustness in PEPCK mutants, *pck-1*(*lf*); *pck-2*(*lf*), during the first 24 h of adulthood (Goncalves et al., 2020). This suggests epidermal PEPCK, within the first 24 h, provides neurons with glycolytic intermediates. However, the rescue did not occur when glucose was fed after day 1 of adulthood in *pck-1*(*lf*); *pck-2*(*lf*) mutants (Goncalves et al., 2020). We expect the lack of behavioral rescue with glucose on day 2 of adulthood may suggest fat synthesis/oxidation increases in the epidermis with age to provide different fuels in the copulatory neuromuscular circuitry (Figure 7C) (Goncalves et al., 2020). This idea is consistent with mammalian studies showing that astrocyte-specific metabolism of medium chain fatty acids contributes ~20% to the neuronal acetyl-CoA pool (Ebert et al., 2003). Given this information, we hypothesize that in aging wild-type males, the epidermis may act similarly to astrocytes by providing fatty acid-derived acetyl-CoA to excitable cells (Figure 7C). Together with the decline in mating fitness of *fat-6*(*lf*); *fat-7*(*lf*) males (Figures 4B and 4D), this suggests well-regulated lipid droplet-dependent fat oxidation during day 2 might delay mating performance decay (Figure 7C).

The *fat-6*(*lf*); *fat-7*(*lf*)mutant males were observed to have increased oxygen consumption on day 1 of adulthood (Figure 2C).While we expect that excessive lipid oxidation can result in premature behavioral decline, we cannot rule out the alternative in which excess saturated fat could accumulate and promote mitochondrial dysfunction and proton leak. Previous work has established the need for unsaturated fat synthesis and incorporation into triacylglycerides as a metabolic option to avoid lipid-based toxicity (Listenberger et al., 2003). Palmitic acid provided by consumed *E. coli* must be expelled or oxidized, otherwise its buildup and metabolism can result in mitochondrial dysfunction and cytochrome *c* release (Hardy et al., 2003). In particular, palmitate induces abnormal levels of phospholipid cardiolipin in the inner mitochondrial membrane. Given that we observed no obvious necrotic or apoptotic cells in *fat-6*(*lf*); *fat-7*(*lf*) mutant males, we suggest that palmitate consumption did not induce severe lipid-based toxicity, and instead day 1 mating behavioral defects are likely a cause of increase ROS production, inefficient oxidative energy production and inappropriate fuel usage by glycolytic-biased tissues (Figure 7D). In addition, while we expect the requirement for day 1 males to prioritize lipid storage for lipolysis on day 2 of adulthood (Figures 7B and 7C), long term lipid deposition, seen in aging hermaphrodites, would most likely result in behavioral dysfunction (Palikaras et al., 2017).

The reduced mating coordination of *fat-6*(*lf*); *fat-7*(*lf*) males is partly due to instability in body posture during spicule insertion. We observed enhanced rhythmic transient calcium activity in several A-class excitatory cholinergic motor neurons, including VA12 and DA7 (Figure 5E). The A-class motor neurons are regulated by premotor AVA interneurons and promote backward movement (Wen et al., 2012; Gao et al., 2018). Conversely, B-class motor neurons are regulated by AVB interneurons and promote forward movement (Wen et al., 2012; Gao et al., 2018). The enhanced transient calcium activity of mutant males (Figure 5E) suggests that neurons involved with their locomotion activate and repolarize faster than wild-type males.

This alteration could lead to locomotive stuttering, causing deficient stabilization during spicule insertion attempts (Figure 4F). Finally, several A- and B-class motor neurons are connected to sensory and motor neurons involved in regulating copulatory-specific locomotion, posture after sensing of the vulva, and spicule insertion attempts (Figure 7A) (Brittin et al., 2021; Cook et al., 2019; Jarrell et al., 2012; Sulston, 1976; Sulston et al., 1980, 1983; Sulston and Horvitz, 1977). Therefore, we suggest that as the wild-type male ages, locomotor coordination of the tail position over the vulva, while executing spicule insertion attempts, requires increases in epidermal *fat-6* expression for maintaining optimal lipid stores and fat oxidation.

Limitations of the study

In the FAT-6:YFP knock-in animals, fluorescence intensity of YFP-tagged FAT-6 reflects similar FAT-6 levels in non-tagged wild-type animals. We acknowledge that the YFP tag might interfere with FAT-6 turn-over and the decreased fluorescent signal during aging might be due to degradation of non-functional protein. Nonetheless, the accumulation of the fluorescently tagged FAT-6 after starvation and refeeding shows that the males are still synthesizing the enzyme. We do not interpret the increase in fluorescent signal as the males are participating in more fat synthesis than in any other life-stage of the male.

We have shown the deficits in mating behavior for *fat-6*(*lf*); *fat-7*(*lf*) and the probable cause of calcium response disruption. We do not discount that the *fat-6*(*lf*); *fat-7*(*lf*) males have multitudes of phenotypes not addressed in this article. Mating motivation is certainly affected in *fat-6*(*lf*); *fat-7*(*lf*) males. The extent to which this impacts mating fitness was not explored fully. We also used oleic acid to alleviate developmental phenotypes but the supplementation effects were variable. We also attest that while we hypothesize membrane composition to be alleviated by oleic acid supplementation, we did not confirm this quantitatively.

STAR★METHODS

Detailed methods are provided in the online version of this paper and include the following:

- KEY RESOURCES TABLE
- RESOURCE AVAILABILITY
  - Lead contact
  - Material availability
  - Data and code availability
- EXPERIMENTAL MODEL AND SUBJECT DETAILS
  - Strains
- METHOD DETAILS
  - Feeding exploring mating assay and Markov modeling
  - Potency, copulation fitness, and endurance assays
  - Expression plasmids and transgenic strains
  - Gonad ablation
  - Quantification of fluorescence
  - RT-qPCR
  - Fixative Nile Red and Oil Red O staining
  - Oleic acid supplementation
  - Oxygen consumption assay
  - Aldicarb assay
- QUANTIFICATION AND STATISTICAL ANALYSIS

SUPPLEMENTAL INFORMATION

Supplemental information can be found online at https://doi.org/10.1016/j.isci.2022.104082.

AUTHOR CONTRIBUTIONS

DECLARATION OF INTERESTS

INCLUSION AND DIVERSITY

REFERENCES

Alfonso, A., Grundahl, K., Duerr, J.S., Han, H.P., and Rand, J.B. (1993). The *Caenorhabditis elegans unc-17* gene: a putative vesicular acetylcholine transporter. Science *261*, 617–619.

Alfonso, A., Grundahl, K., McManus, J.R., Asbury, J.M., and Rand, J.B. (1994a). Alternative splicing leads to two cholinergic proteins in *Caenorhabditis elegans*. J. Mol. Biol. *241*, 627–630.

Alfonso, A., Grundahl, K., McManus, J.R., and Rand, J.B. (1994b). Cloning and characterization of the choline acetyltransferase structural gene (*cha-1*) from *C. elegans*. J. Neurosci. *14*, 2290–2300.

Alqadah, A., Hsieh, Y.W., Schumacher, J.A., Wang, X., Merrill, S.A., Millington, G., Bayne, B., Jorgensen, E.M., and Chuang, C.F. (2016). SLO BK potassium channels couple gap junctions to inhibition of calcium signaling in olfactory neuron diversification. PLoS Genet. *12*, e1005654.

Amtul, Z., Uhrig, M., Rozmahel, R.F., and Beyreuther, K. (2011). Structural insight into the differential effects of omega-3 and omega-6 fatty acids on the production of Abeta peptides and amyloid plaques. J. Biol. Chem. *286*, 6100–6107.

Appel, L.J., Sacks, F.M., Carey, V.J., Obarzanek, E., Swain, J.F., Miller, E.R., 3rd, Conlin, P.R., Erlinger, T.P., Rosner, B.A., Laranjo, N.M., et al. (2005). Effects of protein, monounsaturated fat, and carbohydrate intake on blood pressure and serum lipids: results of the OmniHeart randomized trial. Jama *294*, 2455–2464.

Bargmann, C.I., and Avery, L. (1995). Laser killing of cells in *Caenorhabditis elegans*. Methods Cell Biol. *48*, 225–250.

Baugh, L.R., Kurhanewicz, N., and Sternberg, P.W. (2011). Sensitive and precise quantification of insulin-like mRNA expression in *Caenorhabditis elegans*. PLoS One *6*, e18086.

Ben Arous, J., Laffont, S., and Chatenay, D. (2009). Molecular and sensory basis of a food related two-state behavior in *C. elegans*. PLoS One *4*, e7584.

Brenner, S. (1974). The genetics of *Caenorhabditis elegans*. Genetics *77*, 71–94.

Brittin, C.A., Cook, S.J., Hall, D.H., Emmons, S.W., and Cohen, N. (2021). A multi-scale brain map derived from whole-brain volumetric reconstructions. Nature *591*, 105–110.

Brock, T.J., Browse, J., and Watts, J.L. (2006). Genetic regulation of unsaturated fatty acid composition in *C. elegans*. PLoS Genet. *2*, e108.

Brock, T.J., Browse, J., and Watts, J.L. (2007). Fatty acid desaturation and the regulation of adiposity in *Caenorhabditis elegans*. Genetics *176*, 865–875.

Calhoun, A.J., Tong, A., Pokala, N., Fitzpatrick, J.A., Sharpee, T.O., and Chalasani, S.H. (2015). Neural mechanisms for evaluating environmental variability in *Caenorhabditis elegans*. Neuron *86*, 428–441.

Carlsson, C.M. (2010). Type 2 diabetes mellitus, dyslipidemia, and Alzheimer's disease. J. Alzheimers Dis. *20*, 711–722.

Castelein, N., Hoogewijs, D., De Vreese, A., Braeckman, B.P., and Vanfleteren, J.R. (2008). Dietary restriction by growth in axenic medium induces discrete changes in the transcriptional output of genes involved in energy metabolism in *Caenorhabditis elegans*. Biotechnol. J. *3*, 803–812.

Chen, T.W., Wardill, T.J., Sun, Y., Pulver, S.R., Renninger, S.L., Baohan, A., Schreiter, E.R., Kerr, R.A., Orger, M.B., Jayaraman, V., et al. (2013). Ultrasensitive fluorescent proteins for imaging neuronal activity. Nature *499*, 295–300.

Cherra, S.J., 3rd, Goncharov, A., Boassa, D., Ellisman, M., and Jin, Y. (2020). *C. elegans* MAGU-2/Mpp5 homolog regulates epidermal phagocytosis and synapse density. J. Neurogenet. *34*, 298–306.

Cherra, S.J., 3rd, and Jin, Y. (2016). A two-Immunoglobulin-domain transmembrane protein mediates an epidermal-neuronal interaction to maintain synapse density. Neuron *89*, 325–336.

Cohn, J.A., Cebul, E.R., Valperga, G., Brose, L., de Bono, M., Heiman, M.G., and Pierce, J.T. (2020). Long-term activity drives dendritic branch elaboration of a *C. elegans* sensory neuron. Dev.Biol. *461*, 66–74.

Collins, K.M., and Koelle, M.R. (2013). Postsynaptic ERG potassium channels limit muscle excitability to allow distinct egg-laying behavior states in *Caenorhabditis elegans*. J. Neurosci. *33*, 761–775.

Cook, S.J., Jarrell, T.A., Brittin, C.A., Wang, Y., Bloniarz, A.E., Yakovlev, M.A., Nguyen, K.C.Q., Tang, L.T., Bayer, E.A., Duerr, J.S., et al. (2019). Whole-animal connectomes of both *Caenorhabditis elegans* sexes. Nature *571*, 63–71.

Correa, P., LeBoeuf, B., and García, L.R. (2012). *C. elegans* dopaminergic D2-like receptors delimit recurrent cholinergic-mediated motor programs during a goal-oriented behavior. PLoS Genet. *8*, e1003015.

Cully, D.F., Vassilatis, D.K., Liu, K.K., Paress, P.S., Van der Ploeg, L.H.T., Schaeffer, J.M., and Arena, J.P. (1994). Cloning of an avermectin-sensitive glutamate-gated chloride channel from *Caenorhabditis elegans*. Nature *371*, 707–711.

Deline, M.L., Vrablik, T.L., and Watts, J.L. (2013). Dietary supplementation of polyunsaturated fatty acids in Caenorhabditis elegans. Jove *81*, e50879.

Dickinson, D.J., Ward, J.D., Reiner, D.J., and Goldstein, B. (2013). Engineering the *Caenorhabditis elegans* genome using Cas9-triggered homologous recombination. Nat. Methods *10*, 1028.

Dong, X.X., Wang, Y., and Qin, Z.H. (2009). Molecular mechanisms of excitotoxicity and their

relevance to pathogenesis of neurodegenerative diseases. Acta Pharmacol. Sin *30*, 379–387.

Ebert, D., Haller, R.G., and Walton, M.E. (2003). Energy contribution of octanoate to intact rat brain metabolism measured by 13C nuclear magnetic resonance spectroscopy. J. Neurosci. *23*, 5928–5935.

Escorcia, W., Ruter, D.L., Nhan, J., and Curran, S.P. (2018). Quantification of lipid abundance and evaluation of lipid distribution in Caenorhabditis elegans by Nile Red and Oil Red O staining. Jove *133*, e57352.

Fowler, S.D., and Greenspan, P. (1985). Application of Nile Red, a fluorescent hydrophobic probe, for the detection of neutral lipid deposits in tissue sections. Comparison with Oil Red O. J. Histochem.Cytochem. *33*, 833–836.

Gallagher, T., Bjorness, T., Greene, R., You, Y.J., and Avery, L. (2013). The geometry of locomotive behavioral states in *C. elegans*. PLoS One *8*, e59865.

Gao, S., Guan, S.A., Fouad, A.D., Meng, J., Kawano, T., Huang, Y.C., Li, Y., Alcaire, S., Hung, W., Lu, Y., et al. (2018). Excitatory motor neurons are local oscillators for backward locomotion. Elife *7*, e29915.

Gao, S., and Zhen, M. (2011). Action potentials drive body wall muscle contractions in *Caenorhabditis elegans*. Proc. Natl. Acad. Sci. U S A. *108*, 2557–2562.

Garcia, L.R., Mehta, P., and Sternberg, P.W. (2001). Regulation of distinct muscle behaviors controls the *C. elegans* male's copulatory spicules during mating. Cell *107*, 777–788.

Gems, D., and Riddle, D.L. (2000). Defining wild-type life span in *Caenorhabditis elegans*. J. Gerontol. Ser. A *55*, B215–B219.

Gilleard, J., Barry, D., and Johnstone, I. (1997). Cis regulatory requirements for hypodermal cell-specific expression of the *Caenorhabditis elegans* cuticle collagen gene *dpy-7*. Mol.Cell Biol. *17*, 2301–2311.

Glenn, C.F., Chow, D.K., David, L., Cooke, C.A., Gami, M.S., Iser, W.B., Hanselman, K.B., Goldberg, I.G., and Wolkow, C.A. (2004). Behavioral deficits during early stages of aging in *Caenorhabditis elegans* result from locomotory deficits possibly linked to muscle frailty. J. Gerontol. Ser. A *59*, 1251–1260.

Goldstein, J.L., DeBose-Boyd, R.A., and Brown, M.S. (2006). Protein sensors for membrane sterols. Cell *124*, 35–46.

Goncalves, J., Wan, Y., Guo, X., Rha, K., LeBoeuf, B., Zhang, L., Estler, K., and Garcia, L.R. (2020). Succinate dehydrogenase-regulated phosphoenolpyruvate carboxykinase sustains copulation fitness in aging *C. elegans* males. iScience *23*, 100990.

Goudeau, J., Bellemin, S., Toselli-Mollereau, E., Shamalnasab, M., Chen, Y., and Aguilaniu, H. (2011). Fatty acid desaturation links germ cell loss to longevity through NHR-80/HNF4 in *C. elegans*. PLoS Biol. *9*, e1000599.

Gray, J.M., Hill, J.J., and Bargmann, C.I. (2005). A circuit for navigation in *Caenorhabditis elegans*. Proc. Natl. Acad. Sci. U S A. *102*, 3184–3191.

Greenspan, P., Mayer, E.P., and Fowler, S.D. (1985). Nile Red: a selective fluorescent stain for intracellular lipid droplets. J. Cell Biol. *100*, 965–973.

Gruninger, T.R., Gualberto, D.G., and Garcia, L.R. (2008). Sensory perception of food and insulin-like signals influence seizure susceptibility. PLoS Genet. *4*, e1000117.

Gruninger, T.R., Gualberto, D.G., LeBoeuf, B., and Garcia, L.R. (2006). Integration of male mating and feeding behaviors in *Caenorhabditis elegans*. J. Neurosci. *26*, 169–179.

Guo, X., and García, L.R. (2014). SIR-2.1 integrates metabolic homeostasis with the reproductive neuromuscular excitability in early aging male *Caenorhabditis elegans*. Elife *3*, e01730.

Guo, X., Navetta, A., Gualberto, D.G., and García, L.R. (2012). Behavioral decay in aging male *C. elegans* correlates with increased cell excitability. Neurobiol. Aging *33*, 1483–e1485.

Han, S., Schroeder, E., Silva-Garcia, C., Hebestreit, K., and Mair, W. (2017). Mono-unsaturated fatty acids link H3K4me3 modifiers to *C. elegans* lifespan. Nature *544*, 185–190.

Hardy, S., El-Assaad, W., Przybytkowski, E., Joly, E., Prentki, M., and Langelier, Y. (2003). Saturated fatty acid-induced apoptosis in MDA-MB-231 breast cancer cells. A role for cardiolipin. J. Biol. Chem. *278*, 31861–31870.

Herndon, L.A., Schmeissner, P.J., Dudaronek, J.M., Brown, P.A., Listner, K.M., Sakano, Y., Paupard, M.C., Hall, D.H., and Driscoll, M. (2002). Stochastic and genetic factors influence tissue-specific decline in ageing *C. elegans*. Nature *419*, 808–814.

Hibshman, J.D., Doan, A.E., Moore, B.T., Kaplan, R.E., Hung, A., Webster, A.K., Bhatt, D.P., Chitrakar, R., Hirschey, M.D., and Baugh, L.R. (2017). daf-16/FoxO promotes gluconeogenesis and trehalose synthesis during starvation to support survival. Elife *6*, e30057.

Hills, T., Brockie, P.J., and Maricq, A.V. (2004). Dopamine and glutamate control area-restricted search behavior in *Caenorhabditis elegans*. J. Neurosci. *24*, 1217–1225.

Hodgkin, J.A., Horvitz, H.R., and Brenner, S. (1979). Nondisjunction mutants of the nematode *Caenorhabditis elegans*. Genetics *91*, 67–94.

Huang, J., and Manning, B.D. (2008). The TSC1-TSC2 complex: a molecular switchboard control-ling cell growth. Biochem. J. *412*, 179–190.

Hyun, M., Davis, K., Lee, I., Kim, J., Dumur, C., and You, Y.J. (2016). Fat metabolism regulates satiety behavior in *C. elegans*. Sci. Rep. *6*, 24841.

Ioannou, M.S., Jackson, J., Sheu, S.H., Chang, C.L., Weigel, A.V., Liu, H., Pasolli, H.A., Xu, C.S., Pang, S., Matthies, D., et al. (2019). Neuron-astrocyte metabolic coupling protects against activity-induced fatty acid toxicity. Cell *177*, 1522–1535.e1514.

Jabr, R.I., and Cole, W.C. (1993). Alterations in electrical activity and membrane currents induced by intracellular oxygen-derived free radical stress in Guinea pig ventricular myocytes. Circ. Res. *72*, 1229–1244.

Jarrell, T.A., Wang, Y., Bloniarz, A.E., Brittin, C.A., Xu, M., Thomson, J.N., Albertson, D.G., Hall, D.H., and Emmons, S.W. (2012). The connectome of a decision-making neural network. Science *337*, 437–444.

Johnstone, I.L., and Barry, J.D. (1996). Temporal reiteration of a precise gene expression pattern during nematode development. EMBO J. *15*, 3633–3639.

Kato, H., Sakaki, K., and Mihara, K. (2006). Ubiquitin-proteasome-dependent degradation of mammalian ER stearoyl-CoA desaturase. J.Cell Sci. *119*, 2342–2353.

Kawano, T., Po, M.D., Gao, S., Leung, G., Ryu, W.S., and Zhen, M. (2011). An imbalancing act: gap junctions reduce the backward motor circuit activity to bias *C. elegans* for forward locomotion. Neuron *72*, 572–586.

Kim, E., Sun, L., Gabel, C.V., and Fang-Yen, C. (2013). Long-term imaging of *Caenorhabditis elegans* using nanoparticle-mediated immobilization. PLoS One *8*, e53419.

Kim, K.W., Tang, N.H., Piggott, C.A., Andrusiak, M.G., Park, S., Zhu, M., Kurup, N., Cherra, S.J., Wu, Z., Chisholm, A.D., et al. (2018). Expanded genetic screening in *Caenorhabditis elegans* identifies new regulators and an inhibitory role for NAD(+) in axon regeneration. Elife *7*, e39756.

LeBoeuf, B., and Garcia, L.R. (2012). Cell excitability necessary for male mating behavior in *Caenorhabditis elegans* is coordinated by interactions between big current and ether-a-go-go family K(+) channels. Genetics *190*, 1025–1041.

LeBoeuf, B., Gruninger, T.R., and Garcia, L.R. (2007). Food deprivation attenuates seizures through CaMKII and EAG K+ channels. PLoS Genet. *3*, 1622–1632.

LeBoeuf, B., Guo, X., and García, L.R. (2011). The effects of transient starvation persist through direct interactions between CaMKII and ether-a-go-go K+ channels in *C. elegans* males. Neuroscience *175*, 1–17.

Liang, B., Ferguson, K., Kadyk, L., and Watts, J.L. (2010). The role of nuclear receptor NHR-64 in fat storage regulation in *Caenorhabditis elegans*. PLoS One *5*, e9869.

Listenberger, L.L., Han, X., Lewis, S.E., Cases, S., Farese, R.V., Jr., Ory, D.S., and Schaffer, J.E. (2003). Triglyceride accumulation protects against fatty acid-induced lipotoxicity. Proc. Natl. Acad. Sci. U S A. *100*, 3077–3082.

Liu, P., Chen, B., and Wang, Z.W. (2014). SLO-2 potassium channel is an important regulator of neurotransmitter release in *Caenorhabditis elegans*. Nat. Commun. *5*, 5155.

Liu, P., Ge, Q., Chen, B., Salkoff, L., Kotlikoff, M.I., and Wang, Z.W. (2011). Genetic dissection of ion currents underlying all-or-none action potentials in *C. elegans* body-wall muscle cells. J. Physiol. *589*, 101–117.

Liu, Q., Chen, B., Ge, Q., and Wang, Z.W. (2007). Presynaptic Ca2+/calmodulin-dependent protein kinase II modulates neurotransmitter release by activating BK channels at *Caenorhabditis elegans* neuromuscular junction. J. Neurosci. *27*, 10404–10413.

Liu, Q., and Zhang, J. (2014). Lipid metabolism in Alzheimer's disease. Neurosci. Bull. *30*, 331–345.

Ly, K., Reid, S.J., and Snell, R.G. (2015). Rapid RNA analysis of individual *Caenorhabditis elegans*. MethodsX *2*, 59–63.

Menon, S., Dibble, C.C., Talbott, G., Hoxhaj, G., Valvezan, A.J., Takahashi, H., Cantley, L.C., and Manning, B.D. (2014). Spatial control of the TSC complex integrates insulin and nutrient regulation of mTORC1 at the lysosome. Cell *156*, 771–785.

Miller, K.G., Alfonso, A., Nguyen, M., Crowell, J.A., Johnson, C.D., and Rand, J.B. (1996). A genetic selection for *Caenorhabditis elegans* synaptic transmission mutants. Proc. Natl. Acad. Sci. U S A. *93*, 12593–12598.

Narbonne, P., and Roy, R. (2009). *Caenorhabditis elegans* dauers need LKB1/AMPK to ration lipid reserves and ensure long-term survival. Nature *457*, 210–214.

Nguyen, M., Alfonso, A., Johnson, C.D., and Rand, J.B. (1995). *Caenorhabditis elegans* mutants resistant to inhibitors of acetylcholinesterase. Genetics *140*, 527–535.

Nomura, T., Horikawa, M., Shimamura, S., Hashimoto, T., and Sakamoto, K. (2010). Fat accumulation in *Caenorhabditis elegans* is mediated by SREBP homolog SBP-1. Genes Nutr. *5*, 17–27.

Ochoa, J.J., Pamplona, R., Ramirez-Tortosa, M.C., Granados-Principal, S., Perez-Lopez, P., Naudí, A., Portero-Otin, M., López-Frías, M., Battino, M., and Quiles, J.L. (2011). Age-related changes in brain mitochondrial DNA deletion and oxidative stress are differentially modulated by dietary fat type and coenzyme Q10. Free Radic. Biol. Med. *50*, 1053–1064.

Palikaras, K., Mari, M., Petanidou, B., Pasparaki, A., Filippidis, G., and Tavernarakis, N. (2017). Ectopic fat deposition contributes to age-associated pathology in *Caenorhabditis elegans*. J. Lipid Res. *58*, 72–80.

Perez, C.L., and Van Gilst, M.R. (2008). A 13C isotope labeling strategy reveals the influence of insulin signaling on lipogenesis in *C. elegans*. Cell Metab. *8*, 266–274.

Pino, E.C., Webster, C.M., Carr, C.E., and Soukas, A.A. (2013). Biochemical and high throughput microscopic assessment of fat mass in *Caenorhabditis elegans*. J. Vis. Exp. 50180.

Pradhan, S., Quilez, S., Homer, K., and Hendricks, M. (2019). Environmental programming of adult foraging behavior in *C. elegans*. Curr.Biol. *29*, 2867–2879.e2864.

Rand, J.B., and Russell, R.L. (1985). Molecular basis of drug-resistance mutations in *C. elegans*. Psychopharmacol.Bull. *21*, 623–630.

Reddy, J.K., and Hashimoto, T. (2001). Peroxisomal beta-oxidation and peroxisome proliferator-activated receptor alpha: an adaptive metabolic system. Annu. Rev. Nutr. *21*, 193–230.

Reiner, D.J., Weinshenker, D., Tian, H., Thomas, J.H., Nishiwaki, K., Miwa, J., Gruninger, T., Leboeuf, B., and Garcia, L.R. (2006). Behavioral genetics of caenorhabditis elegans unc-103-encoded erg-like K(+) channel. J. Neurogenet. *20*, 41–66.

Sawin, E.R., Ranganathan, R., and Horvitz, H.R. (2000). *C. elegans* locomotory rate is modulated by the environment through a dopaminergic pathway and by experience through a serotonergic pathway. Neuron *26*, 619–631.

Schedl, T., and Kimble, J. (1988). *fog-2*, a germ-line-specific sex determination gene required for hermaphrodite spermatogenesis in *Caenorhabditis elegans*. Genetics *119*, 43–61.

Schnabel, H., and Schnabel, R. (1990). An organ-specific differentiation gene, *pha-1*, from *Caenorhabditis elegans*. Science *250*, 686–688.

Shi, C., Runnels, A., and Murphy, C. (2017). Mating and male pheromone kill *Caenorhabditis* males through distinct mechanisms. Elife *6*, e23493.

Shi, X., Li, J., Zou, X., Greggain, J., Rødkær, S.V., Færgeman, N.J., Liang, B., and Watts, J.L. (2013). Regulation of lipid droplet size and phospholipid composition by stearoyl-CoA desaturase. J. Lipid Res. *54*, 2504–2514.

Solomon, A., Kivipelto, M., Wolozin, B., Zhou, J., and Whitmer, R.A. (2009). Midlife serum cholesterol and increased risk of Alzheimer's and vascular dementia three decades later. Dement. Geriatr.Cogn.Disord. *28*, 75–80.

Srinivasan, S. (2015). Regulation of body fat in *Caenorhabditis elegans*. Annu. Rev. Physiol. *77*, 161–178.

Steciuk, M., Cheong, M., Waite, C., You, Y.J., and Avery, L. (2014). Regulation of synaptic transmission at the *Caenorhabditis elegans* M4 neuromuscular junction by an antagonistic relationship between two calcium channels. G3 (Bethesda) *4*, 2535–2543.

Sulston, J.E. (1976). Post-embryonic development in the ventral cord of *Caenorhabditis elegans*. Philos. Trans. R. Soc. Lond. B Biol. Sci. *275*, 287–297.

Sulston, J.E., Albertson, D.G., and Thomson, J.N. (1980). The *Caenorhabditis elegans* male: postembryonic development of nongonadal structures. Dev. Biol. *78*, 542–576.

Sulston, J.E., and Horvitz, H.R. (1977). Post-embryonic cell lineages of the nematode, *Caenorhabditis elegans*. Dev. Biol. *56*, 110–156.

Sulston, J.E., Schierenberg, E., White, J.G., and Thomson, J.N. (1983). The embryonic cell lineage of the nematode Caenorhabditis elegans. .Dev. Biol. *100*, 64–119.

Tanaka, T., Ikita, K., Ashida, T., Motoyama, Y., Yamaguchi, Y., and Satouchi, K. (1996). Effects of growth temperature on the fatty acid composition of the free-living nematode *Caenorhabditis elegans*. Lipids *31*, 1173–1178.

Tangney, C.C., Li, H., Wang, Y., Barnes, L., Schneider, J.A., Bennett, D.A., and Morris, M.C. (2014). Relation of DASH- and Mediterranean-like dietary patterns to cognitive decline in older persons. Neurology *83*, 1410–1416.

Teramoto, T., Lambie, E.J., and Iwasaki, K. (2005). Differential regulation of TRPM channels governs electrolyte homeostasis in the *C. elegans* intestine. Cell Metab. *1*, 343–354.

Van Gilst, M.R., Hadjivassiliou, H., Jolly, A., and Yamamoto, K.R. (2005). Nuclear hormone receptor NHR-49 controls fat consumption and fatty acid composition in *C. elegans*. PLoS Biol. *3*, e53.

Vrablik, T.L., Petyuk, V.A., Larson, E.M., Smith, R.D., and Watts, J.L. (2015). Lipidomic and proteomic analysis of *Caenorhabditis elegans* lipid droplets and identification of ACS-4 as a lipid droplet-associated protein. Biochim.Biophys. Acta *1851*, 1337–1345.

Walsh, J.D., Boivin, O., and Barr, M.M. (2020). What about the males? the*C. elegans* sexually dimorphic nervous system and a CRISPR-based tool to study males in a hermaphroditic species. J. Neurogenet. *34*, 323–334.

Wang, Z.W., Saifee, O., Nonet, M.L., and Salkoff, L. (2001). SLO-1 potassium channels control quantal content of neurotransmitter release at the *C. elegans* neuromuscular junction. Neuron *32*, 867–881.

Watts, J.L., and Browse, J. (2000). A palmitoyl-CoA-specific delta9 fatty acid desaturase from *Caenorhabditis elegans*. Biochem.Biophys. Res. Commun. *272*, 263–269.

Wen, Q., Po, M.D., Hulme, E., Chen, S., Liu, X., Kwok, S.W., Gershow, M., Leifer, A.M., Butler, V., Fang-Yen, C., et al. (2012). Proprioceptive coupling within motor neurons drives *C. elegans* forward locomotion. Neuron *76*, 750–761.

Woyda-Ploszczyca, A., and Jarmuszkiewicz, W. (2017). The conserved regulation of mitochondrial uncoupling proteins: from unicellular eukaryotes to mammals. Biochim.Biophys.Acta (Bba) - Bioenerg. *1858*, 21–23.

Wu, S., Cao, X., He, R., and Xiong, K. (2012). Detrimental impact of hyperlipidemia on the peripheral nervous system: a novel target of medical epidemiological and fundamental research study. Neural Regen. Res. *7*, 392–399.

Zhao, J., Zhai, B., Gygi, S.P., and Goldberg, A.L. (2015). mTOR inhibition activates overall protein degradation by the ubiquitin proteasome system as well as by autophagy. Proc. Natl. Acad. Sci. U S A. *112*, 15790–15797.

STAR★METHODS

KEY RESOURCES TABLE

REAGENT or RESOURCE	SOURCE	IDENTIFIER
Chemicals, peptides, and recombinant proteins		
Cis-9-octadecenoic acid	Chem-Impex Int'l. IL. USA	Cat# 01421
Oil Red O	Alfa Aesar, Tewksbury, MA	Cat# A12989
Nile Red	Invitrogen™ Molecular Probes™	Cat# N1142
Polybead polystyrene 0.1 μm microspheres	Polyscience Inc	Cat# 00876
Abamectin	Sigma-Aldrich	Cat# 31732
Aldicarb	Chem Service	Cat# PS-734
Experimental models: Organisms/strains		
fat-6(tm331)	CGC	BX106; WBStrain00004014
fat-7(wa6)	CGC	BX153; WBStrain00004020
fat-5(tm420)	CGC	BX107; WBStrain00004015
fat-5(tm420), fat-7(wa6); rgIs48[P$_{gtl-1}$:fat-6::YFP], him-5(e1490)	This work	CG1823; Upon request
fat-5(tm420), fat-7(wa6); rgIs53[P$_{dpy-7}$:fat-6::YFP], him-5(e1490)	This work	CG1936; Upon request
fat-6(tm331); fat-7(wa6); rgIs50[P$_{gtl-1}$:fat-6:YFP; P$_{dpy-7}$:fat-6::YFP], him-5(e1490)	This work	CG1913; Upon request
fat-6::YFP(rg802); fat-7(wa6), him-5(e1490)	This work	CG1749 Upon request
fat-5(tm420); fat-7(wa36); rgIs49[P$_{unc-17}$:G-CaMP6M::SL2:::RFP]	This work	CG1826; Upon request
Oligonucleotides		
Primers see Table S1	This work	Upon request
Recombinant DNA		
pJG33: *him-5(e1490)* CRISPR/Cas 9 guide RNA plasmid	This work	Upon request
pJG75: *fat-6* 1st exon *fat-6* CRISPR/Cas 9 guide RNA plasmid	This work	Upon request
pJG74: *fat-6* 3'UTR *fat-6* CRISPR/Cas 9 guide RNA plasmid	This work	Upon request
pJG76: P$_{fat-6}$:loxP::fat-6:::YFP::::loxP:::::UTR $_{fat-6}$ CRISPR/CAS9 repair template plasmid.	This work	Upon request
pJG89: Gateway ATTR:loxP::fat-6:::YFP::::loxP:::::UTR $_{fat-6}$ plasmid	This work	Upon request
pJG90: P$_{gtl-1}$: loxP::fat-6:::YFP::::loxP:::::UTR $_{fat-6}$	This work	Upon request
pJG91: P$_{dpy-7}$: loxP::fat-6:::YFP::::loxP:::::UTR $_{fat-6}$	This work	Upon request
pPC64: P$_{unc-17}$: G-CaMP6M::SL2:::RFP	(Correa et al., 2012)	Upon request
Software and algorithms		
Prism V 5.04	GraphPad	https://www.graphpad.com
LabChart 7	ADinstruments	https://www.adinstruments.com/
Metamorph image software	Molecular Devices	https://www.moleculardevices.com/
Other		
ADinstruments Research Powerlab	ADinstruments	https://www.adinstruments.com/

RESOURCE AVAILABILITY

Lead contact

Further information and requests for resources and reagents should be directed to the lead contact L. René Garcia, rgarcia@bio.tamu.edu.

Material availability

Plasmids and worm strains generated in this study are freely available through correspondence with L. René Garcia, rgarcia@bio.tamu.edu.

Data and code availability

- All data reported in this manuscript will be provided upon request.

- The article does not report original code.

- Any additional information required to reanalyze the data reported in this article is available from the lead contact.

EXPERIMENTAL MODEL AND SUBJECT DETAILS

Strains

Male producing *C. elegans* strains, including the wildtype *C. elegans*, contain the *him-5(e1490)* allele and were grown at 20°C on NGM agar plates containing *E. coli* OP50 (Brenner, 1974). Additional strains used in the study were: *pck-2(rg557)* (*pck-2*::YFP knock in) on linkage group (LG) I (Goncalves et al., 2020); *fat-6(tm331)* (Brock et al., 2006), *fat-6*::YFP(*rg802*) (this work) on LG IV; *fat-7(wa36)* (Brock et al., 2006), *him-5(e1490)* (Hodgkin et al., 1979), *fat-5(tm420)* (Brock et al., 2006), *fog-2(q71)* (Schedl and Kimble, 1988) on LGV. Additional strains generated in this study were *fat-6(tm331); fat-7(wa36); rgIs48[P_{gtl-1}:fat-6::YFP].*, *fat-6(tm331); fat-7(wa36); rgIs49[P_{unc-17}:G-CaMP6M::SL2:::RFP].*, *fat-6(tm331); fat-7(wa36); rgIs50[P_{gtl-1}:fat-6::YFp,P_{dpy-7}:fat-6::YFP].*, and *fat-6(tm331); fat-7(wa36); rgIs53[P_{dpy-7}:fat-6::YFP].*

METHOD DETAILS

Feeding exploring mating assay and Markov modeling

Video recordings from the Feeding, Exploring, Mating (FEM) Assay were analyzed on a frame per frame basis. Each frame was taken 15 s apart for 1 h. Each frame was used as a data point and assigned a behavioral state based on the male's position in the FEM assay. For convenience, each behavioral state was given an arbitrary abbreviation. For example, feeding was indicated by the letter A, exploring was indicated by the letter B, and mating was indicated by the letter C.

Time (seconds)	0	15	30	45	60	75	90	105	120	135
Wild-type male	B	B	C	C	C	C	B	B	A	A

The sequences of assigned values were then transformed into three new separate binary sequences. Each binary sequence was representative of a single behavior; the possible behaviors are exploring, feeding, and mating. For each frame, the value of the corresponding behavior the male was performing is 1 with others being 0.

Time (seconds)	0	15	30	45	60	75	90	105	120	135
Wild-type male	B	B	C	C	C	C	B	B	A	A
Feeding	0	0	0	0	0	0	0	0	1	1
Exploring	1	1	0	0	0	0	1	1	0	0
Mating	0	0	1	1	1	1	0	0	0	0

The three binary sequences were then used to calculate the frequency of sustained and shifted behavioral events between neighboring frames. Sustained behavioral events include Feeding-Feeding (FF), Exploring-Exploring (EE), and Mating-Mating (MM). Shifted behavioral events include Feeding-Exploring (FE), Exploring-Feeding (EF), Exploring-Mating (EM), and Mating-Exploring (ME). A behavioral shift of Feeding-Mating and Mating-Feeding was omitted because assay design restricted such a transition. To identify the events, each frame was compared to the next frame. Mathematically, this comparison was done by multiplying the corresponding behavioral values. In the example below, rows 2-4 identify the behavioral states in each frame. Two adjacent frames' behaviors (identified by value 1) are boxed as an example. The next 7 rows demonstrate how the behavioral transitions are identified: the value of each

possible behavioral transition between two frames is calculated by multiplying corresponding behavioral values of these two frames. For example, value of FF at 15 s equals Feeding value at 15 s multiplied by Feeding value at 30 s, which equals zero. In this example, only EM would result in a value of 1 to signify the behavioral transition of exploring to mating.

Time (seconds)	0	15	30	45	60	75	90	105	120	135
Feeding	0	0	0	0	0	0	0	0	1	1
Exploring	1	1	0	0	0	0	1	1	0	0
Mating	0	0	1	1	1	1	0	0	0	0
FF	0	0	0	0	0	0	0	0	1	1
FE	0	0	0	0	0	0	0	0	0	0
EE	1	0	0	0	0	0	1	0	0	0
EF	0	0	0	0	0	0	0	1	0	0
EM	0	1	0	0	0	0	0	0	0	0
MM	0	0	1	1	1	0	0	0	0	0
ME	0	0	0	0	0	1	0	0	0	0

The final step for calculating the choice frequency of behavioral transitions was to sum each row and divide the sum by the total of all the possible behavioral transitions from the specific state (Feeding/Exploring/ Mating). These frequencies were used as transition probabilities in the Markov Model.

												A	B	
												Sum	Model	Calculation
1	FF	0	0	0	0	0	0	0	0	0	1	1	1	A1/(A1+A2)
2	FE	0	0	0	0	0	0	0	0	0	0	0	0	A2/(A1+A2)
3	EE	1	0	0	0	0	0	0	0	0	0	2	0.5	A3/(A3+A4+A5)
4	EF	0	0	0	0	0	0	0	1	0	0	1	0.25	A4/(A3+A4+A5)
5	EM	0	1	0	0	0	0	0	1	0	0	1	0.25	A5/(A3+A4+A5)
6	MM	0	0	1	1	1	0	0	0	0	0	3	0.75	A6/(A6+A7)
7	ME	0	0	0	0	0	1	0	0	0	0	1	0.25	A7/(A6+A7)

For the second order Markov modeling, similar approach was used by analyzing transitions of every three frames instead of two.

In order to verify the Markov Model was similar to the raw data collected, we generated 100 simulations using the model. For each simulation, the sequence of behaviors was sampled using an excel script shown below. First, we use code the behavioral states using numbers: 0 for exploring, 1 for feeding, and −1 for mating. Next, we initiate the first frame as exploring (B1 = 0). For each frame after the first frame, 1–100 is segmented based on the transition probabilities among possible transitions. Then the script generated a random number from −100, determining the behavioral state of the next frame (15 s apart). Below is a sampling and script sample of three frames. For each simulation, the sampling is repeated until the simulated data length reached 1 h (121 frames total).

For example:

A	B
Random #	State
85	0
	1

A	B
Random #	State
21	0
	1
	1

START

B1 is assigned the number 0 to signify exploring. This assignment is only done for the first frame in every model.

A1 is assigned a Random number from 1-100

If A1 >= **90** Then B2 = -1

If A1 >**75**& A1<**90** Then B2 = 1

If A1 <= **75** Then B2 = 0

A1 is assigned a new Random number from 1-100

If B2 = 0

{

If A2 >= **90** Then B3= -1

If A2 >**70**& A2<**90** Then B3 = 1

If A2 <= **70** Then B3 = 0

}

If B2 = 1

{

If A2 >**98** Then B3= 0

If not Then B3 = 1

}

If B2 = -1

{

If A2 >**97** Then B3= 0

If not Then B3 = -1

}

END

For the second order Markov model simulations, a similar approach was applied by swapping the transitions probabilities of the second order Markov model.

A data matrix containing total time spent on feeding, mating, and exploring per worm is used to calculate the proportion of time spent on behaviors. These proportions are then plotted in a diagram shaped as a triangle. As a data point (worm) moves toward any of the vertices the proportion of the behavioral state increases. This allows for the comparison of aged and metabolic mutants using a distribution of total time spent on behaviors.

Potency, copulation fitness, and endurance assays

For the potency assay (Guo et al., 2012), L4 males from non-crowded OP50-spotted NGM plates were separated, 15 males per plate, and allowed to reach adulthood. For assays in which various ages were tested, males were transferred onto new plates on a daily basis, since chronic exposure to accumulated male pheromones has been shown to be harmful (Shi et al., 2017). *pha-1*(*e2123*) hermaphrodites (used as mating partners) were propagated at 15°C (permissive temperature) (Schnabel and Schnabel, 1990). 24 hrs before the assay was conducted, L4 hermaphrodites were transferred from 15°C to 20°C (non-permissive temperature), so that all viable progeny can be identified as cross-progeny. *pha-1* embryos and L1 larva die at 20°C, but cross-progeny, which are heterozygous for *pha-1*, are viable and fertile. To conduct the potency assay at 20°C, one male was paired with one 24-h adult *pha-1* hermaphrodite on a NGM plate containing a 5 mm diameter lawn of OP50. The age of the male could vary depending on the experiment, but the *pha-1* hermaphrodite used was always a 24 hr adult. The mating was scored successful if the plate contained at least 1 cross-progeny.

For the copulation fitness assay (LeBoeuf et al., 2011), L4 males from non-crowded OP50-spotted NGM plates were separated, 15 males per plate, and allowed to reach adulthood. For assays in which various ages were tested, males were transferred onto new plates on a daily basis. L4 *fog-2*(*q71*) females, which do not make sperms, were picked from their male siblings 24 h before conducting the assay (Schedl and Kimble, 1988). On the day of the assay, a 24 hr adult *pck-2* (*rg557*) male containing a CRISPR/Cas9 YFP translational fusion knock-in *pck-2*::YFP (the wild-type control) and one unmarked 24 hr adult male (the queried male) were paired with a virgin *fog-2*(*q71*) female on a 5 mm diameter OP50 lawn. The paired males were allowed to mate for 3 hrs before being removed. In the following days, the female's progeny were screened for either the presence or lack of YFP to determine paternity. Plates containing both fluorescent and non-fluorescent progeny were not counted, as paternity was shared between the competing males.

The copulation endurance assay, modified from previous work, measures the kinetics of male mating and the number of females impregnated, across the first 3 days of adulthood (Goncalves et al., 2020). L4 males from non-crowded OP50-spotted NGM plates were separated, 15 males per plate, and allowed to reach adulthood. L4 *fog-2*(*q71*) females were picked 24 hrs before conducting the assay. On the day of the assay, one day 1 adult male was paired with 10 day 1 adult females. Every 12 hrs, egg-containing females were counted and replaced with virgin females, similarly aged to the male. The male and the 10 females were then transferred to a new plate and allowed to mate for another 12 hrs. This was repeated for 72 hrs.

The copulation endurance assay was analyzed in multiple ways. For example, we quantified the percent of males who mated per time point. For a male to be considered successful, it would have had to mate into a single female during the specific time point. To quantify the number of females impregnated, we summed the total number of females impregnated at a time point across all males.

Expression plasmids and transgenic strains

The primers used in this work are listed in Table S1. To generate the *fat-6* CRISPR/Cas 9 guide RNA plasmid pJG74 and pJG75, the 19 bp guide RNA sequence to the *fat-6* 3'untranslated region (UTR) (5'-cggaacgcccggggtttcc -3') and 5' 1st exon (5'-gagacgcaatatctcgccg -3'), was added to the CRISPR/Cas 9 guide RNA/ enzyme plasmid pDD162 (Dickinson et al., 2013) using PCR and the primers, forfat62cas9: cggaacgcccggggtttccgttttagagctagaaatagcaagt, forfat6cas9: gagacgcaatatctcgccggttttagagctagaaatag caagt, and sgRNA(universal)REV: caagacatctcgcaatagg. Sequence errors were checked using primer SEQpDD122-sgRNA(universal): ctgctgagacctgaaaatagc.

The *fat-6* repair template used for CRISPR/Cas 9-mediated recombination was generated by PCR-amplifying from genomic DNA a ∼ 4.5 kilo base pair (kb) fragment containing the promoter and gene. This fragment was amplified using the primers ForATTBfat6Prom: ggggacaagtttgtacaaaaaagcaggctaccatcttcatcaatcttgcgccac gaacc and Revfat6ATTB: ggggaccactttgtacaagaaagctgggtcatgattgattttcctcgttgaatatcacat. The fragment was then recombined into pDG15 by Invitrogen BP clonase to generate pJG45. To fuse YFP to the *fat-6* gene, a second recombination occurred between pJG45 and pGW322YFP by Invitrogen LR clonase to generate pJG61. The YFP was not directly fused by the recombination reaction and so the primers linfat6yfp: atgagtaaaggaga agaacttttccactggagttgtccca and reversefat6nostop: catgattgattttcctcgttgaatatcacatccatgattggatac were used to correct the frameshift to generate pJG62. To create greater homology, we PCR-amplified the *fat-6* 3′ UTR using primers fat6forutryfp: tggatgaactatacaaataggatactgttccgtattcactcaaataagag and fat6revutrunc54: gcacgggcg cgagatgctgagcgtacttctcgtttatttcacatttgacttac. We also linearized pJG62 using primers fat6forlinpjg62: gaa ataaacgagaagtacgctcagcatctcgcgcccgtgcctc and fat6revlinpjg62: agtgaatacggaacagtatcctatttgtatagttcat ccatgccatgtgtaatcccag. Using the In-Fusion HD-cloning, we fused the PCR fragment *fat-6* 3′ UTR to the last codon of YFP in the plasmid pJG62 generating pJG63. A single loxp site were added to pJG63 by using the primers fat 6for5primeloxp: accatatacgaagttatgacatcgagtagtcgaacatttcatgtcaactgtc and fat6rev5primeloxp: accatata cgaagttatgctgatcacattgatcagaactgataagacgacac. Quick ligase was used to join homologous ends to generate pJG64. This was repeated for the second loxp site using primers fat6for3primeloxp: accatatacgaagttatg atactgttccgtattcactcaaataagag and fat6rev3primeloxp: accatatacgaagttatctatttgtatagttcatccatgccatgtgtatc. Quick ligase was used to join homologous ends to generate pJG65. The PAM sites located at the 3′ UTR were mutated using primers fat6for3primepammut: gtttcccatatcacagacgaaccccac and fat6rev3primepammut: cccgggcgttccggtttgcaaatc. Quick ligase was used to join homologous ends to generate pJG66. The PAM sites located at the 5′ 1st exon were mutated using primers fat6for5primepammut: gacgcaatatctcgccgtagatccaaatg and fat6rev5primepammut: tctgggccgccgtccttctcaatc. DNA ligase was used to join homologous ends to generate pJG67. Plasmids were sequenced and repaired for mutations that arose during the construction, to generate pJG76.

The plasmid pJG76 had the *fat-6* promoter removed and the Invitrogen Gateway ATTR cassette B was cloned in using In-Fusion HD-cloning creating pJG89. The cassette was PCR-amplified using primers forfat6attr1ccdb: tgcctgcaggtcgactctagatcaaacaagtttgtacaaaaaagctgaac and revccdbattr2fat-6: tgtttgaacgagttttttaccgtcatacca ctttgtacaagaaagctgaac. pJG76 was linearized using primers revlinfat6attr1: tcagctttttttgtacaaacttgtttgatctagag tcgacctgcaggcatgcaagcttatc and forlinfat6attr2: cttgtacaaagtggtatgacggtaaaaactcgttcaaacatcgcaaaaaagat tgag. For intestinal expression, the gateway entry plasmid pBL63 (LeBoeuf et al., 2007) was used to recombine in the *gtl-1* promoter (Teramoto et al., 2005) to generate pJG90. For epidermal expression, the gateway entry plasmid pXG76 was used to recombine in the *dpy-7* promoter (Gilleard et al., 1997) to generate pJG91. Injection mixes, containing 50 ng/μL of pJG90 and/or pJG91 and up to 150 ng/μL of pUC18 filler DNA, were injected into the germline of *fat-7(lf); fat-5(lf)* hermaphrodites. Stable transgenic lines that heritably transmitted YFP fluorescence were then used to generate UV-induced integrated lines: *fat-7(wa36); fat-5(tm420); rgIs48 [P_{gtl-1}:fat-6::YFP]*, *fat-7(wa36); fat-5(tm420); rgIs53[P_{dpy-7}:fat-6::YFP]*, and *fat-7(wa36); fat-5(tm420); rgIs50[P_{gtl-1}:fat-6::YFP , P_{dpy-7}:fa- t-6::YFP]*. The integrations were not mapped. Then *fat-7(wa36); him-5(e1490) males were crossed into fat-7(wa36); fat-5(tm420); rgIS48 [P_{gtl-1}:fat-6::YFP] to generate fat-7(wa36); him-5(e1490); rgIS48[P_{gtl-1}:fat-6::YFP]. The fat-7(wa36); him-5(e1490); rgIs48[P_{gtl-1}:fat-6::YFP] males were then crossed into fat-6(tm331); fat-7(wa36); him-5(e1490) to generated fat-6(tm331); fat-7(wa36); him-5(e1490); rgIs48[P_{gtl-1}:fat-6::YFP]. Similarly, fat-6(tm331); fat-7(wa36); him-5(e1490) males were crossed into fat-7(wa36); fat-5(tm420); rgIs50[P_{gtl-1}:fat-6::YFP, P_{dpy-7}:fat-6::YFP] and fat-7(wa36); fat-5(tm420); rgIs53[P_{dpy-7}:fat-6::YFP] to generate fat-6(tm331); fat-7(wa36); him-5(e1490); rgIs50[P_{gtl-1}:fat-6::YFP, P_{dpy-7}:fat-6::YFP] and rgIs53[P_{dpy-7}:fat-6::YFP], respectively.* The plasmid pPC64 containing the *unc-17* promoter driving G-CaMP6M:SL2::RFP (Correa et al., 2012) was injected and UV-integrated to generate *rgIs49[P_{unc-17}:G-CaMP6M::SL2:::RFP]*; the integration was not mapped. *rgIs49* was then crossed into the *fat-6(tm331); fat-7(wa36); him-5(e1490)* mutant background.

The CRISPR/Cas9 plasmids and protocols, established in Dickinson et al. (2013), were used in this report (Dickinson et al., 2013). To generate the genomic *fat-6*::YFP knock-in, a hundred 5- to 10-hour-old adult *N2* hermaphrodites were microinjected with 50 ng/μL of the CRISPR/CAS9 plasmids pJG74 and pJG75, and 50 ng/μL the *fat-6*::YFP repair template pJG76. In the F2 and F3 generation, fluorescent animals were picked and analyzed by PCR and sequencing to verify homologous recombination between the repair template and the genomic *fat-6* locus. In this work, the *fat-6(rg802)*::YFP knock-in allele is referred to as *fat-6*::YFP. We also validated the knock-in of loxP by expressing *Pges-1:Cre,*and we observed a reduction

in FAT-6::YFP between 54-60% during larval development. The remaining FAT-6:YFP was highly mosaic and did not result in obvious mutant phenotypes.

The *him-5*(*e1490*)mutation is a G-to-A transition affecting the splice acceptor site at the start of exon 4 (or at the end of intron 3). To generate the *him-5*(*e1490*) CRISPR/Cas 9 guide RNA plasmid, the 19 bp guide RNA sequence to the *him-5* (*e1490*) slice acceptor site (5'-cggaacgcccggggtttcc -3') was added to the CRISPR/Cas 9 guide RNA/enzyme plasmid pDD162 using PCR and the primers, ForHim5Cas9sgRNA: ttattttccag gcaaagctcgttttagagctagaaatagcaagt and sgRNA(universal)REV: caagacatctcgcaatagg to create pJG33. Sequence errors were checked using primer SEQpDD122-sgRNA(universal): ctgctgagacctgaaaatagc. The repair template used was the oligo him-5(e1490)Oligo: cctttctatgttagtaatttttaaaaacatggaattttactgatta ttttccaagctaagctccgtaaagctaactccaagtattcctcaaagcccaaagaaagaga.

To generate the mutation of *him-5*(*e1490*), a hundred 5- to 10-hour-old adult *fat-7*(*lf*) hermaphrodites were microinjected with 50 ng/μL of the CRISPR/Cas9 plasmids, and 50 ng/μL of the oligo repair template. Others have shown the use of an oligo 161 bp long for CRISPR generated *him-5*(*e1490*) (Walsh et al., 2020). In the F2 and F3 generation, males were picked and allowed to mate into *fat-7*(*lf*) hermaphrodites. We verified the *him-5*(*e1490*)mutation by PCR and sequencing.

Gonad ablation

Following previously established protocols (Bargmann and Avery, 1995), we laser-ablated the Z1, Z2, Z3, and Z4 gonad precursor cells (Sulston et al., 1983) in early *fat-6*(*rg802*) L1 animals. During the ablation, we immobilized the animals with 5% agarose pads infused with 10 mM sodium azide. 3 L1 worms were put on the pad and ablated at a time. The total time worms on the pads were controlled to be less than 10 min to limit unspecific damages to the animals. At L4, we separate the males from the hermaphrodites and quantified the day 1 and day 2 adults male's intestinal FAT-6::YFP fluorescence.

Quantification of fluorescence

Digital images of animals were obtained using a Yokogawa CSU-X1 Spinning Disk Unit (Andor Technology, CT USA) mounted on an Olympus IX81 microscope. To image FAT-6::YFP fluorescence, animals were anesthetized using abamectin (Sigma-Aldrich, Cat# 31732) (Cully et al., 1994). A 50 mg/mL DMSO stock of abamectin was diluted in M9 buffer to the working concentration of 250 μg/mL. Worms were soaked in 1-5 μL of solution. Generally, 1–2 min elapsed before the worms became paralyzed. Nile Red-stained and YFP-containing animals were imaged using the 10X objective for a full body perspective, and 100X objective for individual cell resolution.

Metamorph image software (version 7.8.0.0., Molecular Devices) was used to quantify average pixel intensity of a Region-Of-Interest (ROI). To quantify FAT-6::YFP, a series of rectangular ROIs were drawn across the entire intestine. The average pixel intensity was determined for each ROI and a single average of all ROIs was calculated for the whole intestine. If the intestine was analyzed into differing segments, then only the average pixel intensity for a specific set of ROI was averaged. For example, the anterior intestine was composed of the first ∼5 intestinal rectangular ROIs. The pixel intensity was averaged for each ROI and then a single average was calculated from the subset.

For calcium imaging, we collected G-CaMPV6 and RFP fluorescence images from un-anesthetized, immobilized males using a Dual View Simultaneous Image Splitter (Photometrics, AZ) and a Hamamatsu ImagEM Electron multiplier (EM) CCD camera. To restrain the animals, un-anesthetized males were mounted between a coverslip and a 10% Noble agar pad containing Polybead polystyrene 0.1 μm microspheres (Polyscience Inc, Cat# 00876). The recordings were analyzed in SimplePCI software (version 6.6.0.0, Hamamatsu) and Microsoft Excel.

Because the male was restrained on the agar pad and was not mating, we could not observe changes in the SPC/PCB/PCC sex motor neurons. However, we did observe changes in the posterior cholinergic motor neurons in the ventral cord, including CA8, VB11, DB7, AS10, DA7, CA9, VA11, AS11, and VA12, as the male struggled under restraint. Given the dynamic changes seen, we generated ROIs of equal areas around the ventral cord neurons using Simple PCI software. These neurons were never obscured by other tissues, but some ventral cord neurons were mosaic in that they did not always express the calcium sensor. As such, we labeled the neurons appropriately and kept track of their location. ROIs were used to measure the

background signal and fluorescent signals from the green and red emission channels. Males were immobilized, so the ROIs remained in position throughout the time course; but if there was movement, ROIs were adjusted appropriately. The mean pixel intensity was then transferred into Microsoft Excel and background signals were subtracted from neuronal signals.

Wavelength was approximated using Prism software. Amplitude was measured by taking the difference between a local max and local min of every individual peak. To quantify signal duration, we used the average fluorescence across time to set a threshold. Each male had an individual calcium wave with a unique threshold. Using the threshold as the baseline, we then measured the distance between both sides of a single peak. Each male had 3 peaks quantified.

Photo-bleaching artifacts caused unwanted fluorescent changes. A higher rate of RFP photo-bleaching, relative to minimal G-CaMP6 photo-bleaching, required appropriate signal correction. We modeled the RFP bleaching using a one-phase decay curve and fitted it over the data points using Prism software. The fitted curve described unwanted changes in fluorescent. For every frame the fitted curve was used to correct the background subtracted red channel mean pixel intensity (MPI). The MPI value was divided by the fitted red value to give a correction value. This was then applied to the green channel MPI for the respective frame. The resulting data solely reflected changes in calcium.

The expression levels of G-CaMP6 differed between wild-type and *fat-6*(*lf*); *fat-7*(*lf*) males. To quantify the amplitude of the calcium signal we corrected for transcriptional activity of the promoter of a vesicular acetylcholine transporter (divide by the mean difference in expression).

RT-qPCR

The sequences for primers that anneal to the metabolic genes *sod-4*, *ctl-1*, T20H4.5, *cco-1*, *ech-2*, and *fat-5* were described previously (Castelein et al., 2008). The sequences for forward primers that anneal to *unc-103* isoforms D and A are forunc103c: cactagtggcaagatcggga and forunc103i: tgcgtgcggttctatcactt, respectively; the reverse primer used to amplify both isoforms is revunc103universal: aacatcggcgccaag tgata. When searching through wormbase.org, we found discrepancies with previously published work (Reiner et al., 2006). Of note for this work, wormbase.org incorrectly labels *unc-103* isoforms A and D as I and C, respectively. The *unc-103* primer pair that amplifies all *unc-103* isoforms are 2qPCRunc-103F: ttcagtgtctccaacaacgg and 2qPCRunc-103R: tgttctgcattcgttccatttg. The primer pairs to amplify *egl-2* are 2qPCRegl-2F: gagtaaaccgaagagacctcc and 2qPCRegl-2R: tccattccccaacttgtacg. The primer pair to amplify *slo-1* are F1-qPCRslo1ex11: ctggtgtaagcagtgtcatgac and qPCRslo1ex12-1R: ggccgctgtcgagtgtttg. Primers for *unc-15* are unc-15F07A5.7qPCRF: gaagaagaagtaccaggctgagatcg and unc-15F07A5.7qPCRF: gaagaag aagtaccaggctgagatcg.

The RT-qPCR protocol for making cDNA from a single worm was adapted from (Ly et al., 2015). L4 males were picked from hermaphrodites and kept at 10 to 15 males per plate. The next day, males displaying a protracted constitutive spicule phenotype (Prc phenotype) were separated from normal behaving males. A single microliter of lysis solution (5 mM Tris pH 8, 0.5% triton X-100, 0.5% Tween 20, 0.25 mM EDTA; 1 mg/mL Protease K) was added to the cap of a PCR tube. Using an eye lash, a single male was transferred to the lysis buffer. Using a sharpened platinum pick, we cut the worm in the lysis buffer. Each male can be processed in less than 5 min. Then samples were frozen at −70°C, and incubated at 65°C for 20 min, followed by 85°C for 5 min. Once the lysis was complete, 10 μL of Turbo DNAse I solution (8 μL nucleasefree water, 1 μL 10X Turbo DNAse I buffer, 1 μL Turbo DNAse I) was added, and the sample was incubate at 37°C for 20 min. We then added 2 μL of Turbo DNAse I inactivation beads and incubated 5 min. We spun down and remove 10 μL of the lysed worm solution. We then added 1 μL of dNTP and 1 μL of oligo dT or gene-specific primers (for *unc-103* transcripts: 2qPCRunc-103R: tgttctgcattcgttccatttg; for *slo-1* transcripts: Slo1ex17r: taaatctgctcgagatagcggggagc; and for *egl-2* transcripts: cDNAegl2D: tcatatccgtgttcttgtcgga ggacgggc) and incubated at 65°C for 5 min; the sample was put on ice for 1 min to anneal. Finally, we added 10 μL of the RT solution containing (2 μL 10X RT buffer; 4 μL 25 mM MgCl2, 2 μL 0.1 M DTT, 1 μL RNAse out; 0.5 μL Superscript II RT; 0.5 μL nuclease-free water) and incubated at 42°C for 50 min and 70°C for 15 min.

Fixative Nile Red and Oil Red O staining

The Nile Red staining was adapted from (Pino et al., 2013). L4 males from non-crowded OP50-spotted NGM plates were separated 15 males per plate and allowed to reach adulthood. Aging males were transferred

onto new plates on a daily basis. On the day of the assay 30–50 males were transferred using 25 μL of PBS with 0.01% triton X-100 (Sigma-Aldrich) to a 1.5 mL Eppendorf tube. Animals were then fixed using 150 μL of 40% isopropanol and incubated at room temperature for 3 min. During this incubation, 1 mL of Nile Red (Invitrogen™ Molecular Probes™, Cat# N1142) stain was prepared using 6 μL Nile Red stock solution (0.5 mg/mL in acetone) per 1 mL of 40% isopropanol. Males were pelleted by centrifugation and the supernatant was aspirated leaving 25 μL. To each worm pellet, 150 μL of Nile red staining solution was added, and males were stained in the dark for 2 h. Males were then collected by centrifugation and the supernatant was aspirated leaving 25 μL. Males were incubated with 150 μL of PBS with 0.01% triton X-100 in the dark for 30 min. Males were centrifuged and the supernatant was aspirated leaving 25 μL. Before imaging 1-5 males were transferred to a glass slide with 2% noble agar pad.

Males were imaged on a Yokogawa CSU-X1 Spinning Disk Unit mounted on an Olympus IX81 microscope (514 nm laser excitation/540 nm emission) using a 10X objective. Metamorph imaging software was used to quantify the average intensity of intestinal neutral lipid stores. To quantify Nile Red staining a series of rectangular ROIs were drawn across the entire intestine. The average pixel intensity was determined for the first 5 ROIs and a single average of all ROIs was calculated. Nile Red staining was occluded by hermaphrodite eggs therefore we treated hermaphrodites and males similarly by only calculating average intensity using the first five segmented ROIs.

Oil Red O staining was adapted from (Escorcia et al., 2018). On the day of the assay, males were washed of bacteria using PBS with 0.01% triton X-100 and pelleted in a 1.5 mL Eppendorf tube. The PBS 0.01% triton X-100 solution was removed and animals were then fixed using 40% isopropanol and incubated at room temperature for 3 min. Worms were pelleted and the 40% isopropanol was removed. A 5 mg/mL stock solution of Oil Red O in 100% isopropanol (Alfa Aesar, Tewksbury, MA Cat# A12989) was diluted 3 parts stock Oil Red O to 2 parts water to make a 60% isopropanol working stock. The working stock was filtered using a 2 μm filter and ∼500 μL of Oil Red O was added to the animals; the animals were stained in the dark for ∼2 h. Males were then collected by centrifugation and males were washed with PBS with 0.01% triton X-100 for 30 min. 1–5 males were transferred to a glass slide with 2% noble agar pad. Grey scale digital images of animals were obtained using a Hamamatsu ImagEm camera mounted to an Olympus BX51 microscope (Olympus Corporation, Tokyo Japan). Using Metamorph imaging software, grey scale images were inverted so that dark pixels were now depicted as luminous pixels. The background was subtracted from the images. To quantify Oil Red O staining, a series of rectangular ROIs were drawn across the entire intestine. The average pixel intensity was determined for the ROIs and a single average of all ROIs was calculated.

Oleic acid supplementation

Oleic acid supplementation was adapted from (Brock et al., 2006; Deline et al., 2013).Cis-9-octadecenoic acid (oleic acid; Chem-Impex Int'l. IL. USA Cat# 01421) was added at a final concentration of 0.3 mM to liquid NG media containing 0.1% tergitol (NP40).E. coli OP50 was added to the media and grown at 37°C with shaking aeration overnight to saturation. The next day, 100-200 μL of bacterial culture was spotted on a 5 cm diameter NGM plate and allowed to dry. Worms were added on the same day and progeny were transferred to newly prepared NGM plates with oleic acid-supplemented E. coli OP50 every 24 h. We did not observe any obvious behavioral alterations in the day 1 oleic acid-fed male's mating ability (mating potency is 95%; n = 20 males). However, excessive chronic feeding of oleic acid to wild-type males does have deleterious effects in older animals. On day 2, the mating potency dropped (55%; n = 20 males), and on day 3, the mating potency was 35%; n = 20.

Oxygen consumption assay

ADinstruments Research Powerlab (Colorado Springs, CO), equipped with an oxygen microelectrode (Microelectrodes, Inc. Bedford, NH) records voltage as a proxy for changes in dissolved oxygen in solution. Increase in voltage measures approximate decreases in dissolved oxygen; decrease in voltage measures approximate increases in dissolved oxygen. Fifty day 1 adult males, for each independent sample, were added to 50 μL of S-basal buffer (0.1M NaCl, 0.05 M KH_2PO_4, 0.005 mg/mL cholesterol) in 3 mL glass conical test tubes. 5 mm of the microelectrode tip was submerged in the S-basal. The electrode voltages were recorded for 20 min using LabChart 7 (ADinstruments). Recordings of the first 5 min were trimmed before 10 min of analysis to allow for equilibration of the system; the system must be equilibrated due to acclimation of the electrode to the buffer (from air to liquid).

Aldicarb assay

Aldicarb (Chem Service, PA; Cat# PS-734) was prepared in distilled water and kept frozen at −20°C as 100 mM. Aldicarb was then diluted with concentrations ranging from 5-15 mM. Media containing 500 μL of NGM with aldicarb was allowed to solidify in a Pyrex round-bottom, 3-well titer dish. Then ten day 1 adult virgin males were transferred to the solid media. Males were watched for 10 min and scored if they protracted their spicules for more than 10 s.

QUANTIFICATION AND STATISTICAL ANALYSIS

Statistical p values were computationally determined using Prism software (version 5.04, GraphPad).